

Hyperbolic Gaussian Blurring Mean Shift: A Statistical Mode-Seeking Framework for Clustering in Curved Spaces

Arghya Pratihar¹, Arnab Seal², Swagatam Das^{1*}, Inesh Chattopadhyay²

¹Electronics and Communication Sciences Unit, Indian Statistical Institute, Kolkata, India.

²Indian Statistical Institute, Kolkata, India.

*Corresponding author(s). E-mail(s): swagatam.das@isical.ac.in;

Contributing authors: arghyapratihar24@gmail.com; arnabseal37@gmail.com;
ineshchattopadhyay@gmail.com;

Abstract

Clustering is a fundamental unsupervised learning task for uncovering patterns in data. While Gaussian Blurring Mean Shift (GBMS) has proven effective for identifying arbitrarily shaped clusters in Euclidean space, it struggles with datasets exhibiting hierarchical or tree-like structures. In this work, we introduce HypeGBMS, a novel extension of GBMS to hyperbolic space. Our method replaces Euclidean computations with hyperbolic distances and employs Möbius-weighted means to ensure that all updates remain consistent with the geometry of the space. HypeGBMS effectively captures latent hierarchies while retaining the density-seeking behavior of GBMS. We provide theoretical insights into convergence and computational complexity, along with empirical results that demonstrate improved clustering quality in hierarchical datasets. This work bridges classical mean-shift clustering and hyperbolic representation learning, offering a principled approach to density-based clustering in curved spaces. Extensive experimental evaluations on 11 real-world datasets demonstrate that HypeGBMS significantly outperforms conventional mean-shift clustering methods in non-Euclidean settings, underscoring its robustness and effectiveness.

Keywords: Clustering, Hyperbolic Geometry, Poincaré Ball, Blurring Mean-Shift.

1 Introduction

Clustering is a fundamental unsupervised learning paradigm that organizes data into groups of similar entities, thereby revealing latent patterns and structural regularities within complex datasets. It enables the discovery of meaningful associations without requiring predefined class labels. Over the years, a broad spectrum of clustering algorithms has been developed, broadly categorized into *hard* and *soft* clustering methods. In hard clustering, each data point is assigned to a single cluster, whereas soft clustering allows points to belong to multiple clusters to varying degrees.

Hard clustering techniques encompass several major families: *center-based*, *hierarchical*, *distribution-based*, and *density-based* methods. Center-based approaches—such as k -means [1], spectral clustering [2], and kernel k -means [3] measure similarity through proximity to cluster centroids. Hierarchical approaches, including hierarchical clustering [4] and agglomerative clustering [5], assume that data points exhibiting closer pairwise similarities belong to the same cluster. Distribution-based methods, such as Expectation–Maximization (EM) for Gaussian Mixture Models [6] and its robust variants [7], model the data through underlying probabilistic distributions. Density-based approaches like DBSCAN [8], HDBSCAN [9], and Mean Shift [10] instead infer cluster structure by identifying regions of high data density in the feature space.

Most of the aforementioned algorithms require the number of clusters to be specified *a priori*. Among them, the **Mean Shift** algorithm has received significant attention because of its non-parametric, **mode-seeking** nature; it adaptively locates regions of high density without assuming a fixed number of clusters or a particular cluster shape. In particular, the **Gaussian Blurring Mean Shift (GBMS)** algorithm [11]

provides a smooth iterative framework for finding the modes of an underlying density in Euclidean space by progressively moving data points toward Gaussian-weighted means. This elegant formulation has found widespread success in computer vision, image segmentation, and manifold learning, owing to its simplicity, non-parametric flexibility, and theoretical grounding in kernel density estimation.

Despite its strengths, traditional Euclidean mean-shift variants encounter difficulties when applied to datasets that exhibit *hierarchical or tree-like structures*, such as taxonomies, linguistic ontologies, or social and biological networks. Such data are more naturally represented in **hyperbolic space**, where the geometry grows exponentially and inherently accommodates hierarchical expansion. Recent advances in hyperbolic representation learning have shown that embeddings in hyperbolic space can capture hierarchical relationships far more compactly than Euclidean embeddings, often requiring fewer dimensions while maintaining minimal distortion of the underlying structure.

To overcome these limitations, we introduce the **Hyperbolic Gaussian Blurring Mean Shift** (HypeGBMS) algorithm, which generalizes the GBMS procedure from Euclidean space to the **Poincaré ball model** of hyperbolic geometry. The key idea is to replace Euclidean distance computations with hyperbolic distances and to adapt the mean-shift update rule through **Möbius-weighted means**, thereby ensuring consistency with the non-Euclidean geometry of the underlying space. By adjusting the curvature parameter of the Poincaré ball, HypeGBMS provides a principled and flexible mechanism for **mode-seeking clustering** in hyperbolic space while preserving the desirable density-seeking behavior of the original GBMS. A major strength of the proposed framework lies in ensuring that all iterative updates remain confined to the Poincaré ball, thus maintaining the integrity of the hyperbolic manifold throughout the clustering process.

The Poincaré ball metric naturally preserves hierarchical relationships through its *exponential distance scaling* and *negative curvature*, which contrast sharply with the linear geometry of Euclidean space. As distances increase exponentially with displacement from the origin, hyperbolic space efficiently represents hierarchical data; levels of a hierarchy are automatically well-separated, enhancing cluster discernibility. Furthermore, the *conformal property* of the Poincaré model preserves local angles and relative positioning, thereby retaining geometric fidelity when clustering complex, high-dimensional datasets. These properties make hyperbolic geometry especially well-suited for discovering latent hierarchies and non-Euclidean relationships where conventional Euclidean methods often fail.

Contributions. The main contributions of this work are as follows:

1. We propose **HypeGBMS**, a hyperbolic extension of Gaussian Blurring Mean Shift that embeds data within the Poincaré ball and ensures that all mode updates remain consistent with its geometric constraints.
2. We demonstrate that this formulation effectively captures hierarchical data structures and improves clustering performance in domains where Euclidean methods are inadequate.
3. We provide a detailed convergence and consistency analysis, along with a computational complexity study, and include supporting proofs and derivations in the Appendix.

In summary, this study bridges the conceptual divide between classical **mode-seeking** mean-shift clustering and modern **hyperbolic representation learning**, presenting a unified statistical framework for clustering in both flat and curved geometries.

2 Related Works

Clustering methods have evolved across diverse algorithmic paradigms, with mean-shift and its extensions forming an important class of non-parametric density-based techniques. The *mean-shift algorithm* estimates modes of an underlying probability density function by iteratively shifting data points toward regions of higher density. Carreira-Perpiñán [12] provided a comprehensive review of mean-shift algorithms, including Gaussian Blurring Mean-Shift (GBMS), hierarchical variants, and scale-space clustering approaches that extend its applicability across multiple domains. To improve computational efficiency in high-dimensional settings, Chakraborty et al. [13] proposed feature-weighted GBMS for fast nonparametric clustering, demonstrating scalability without sacrificing clustering quality.

On a different note, hyperbolic geometry has gained traction for representing data with hierarchical or tree-like structures. Unlike Euclidean embeddings, which suffer from distortion when encoding exponentially expanding hierarchies, hyperbolic models provide a natural geometric prior. Earlier work, such as the Hierarchically Growing Hyperbolic SOM [14], explored hyperbolic topology for large-scale data exploration. More recently, hyperbolic graph embeddings have been applied to biological and neurological networks, where hierarchical structure is intrinsic [15]. Hyperbolic kernels and Poincaré embeddings have also been introduced to improve representation learning by aligning learning objectives with hyperbolic curvature [16].

Building upon this foundation, several methods have bridged *clustering* with *hyperbolic embeddings*. Chami et al. [17] developed hyperbolic hierarchical clustering techniques that recover tree-like structures directly from embeddings, enabling robust inference of latent hierarchies. Similarly, Zhao et al. [18] explored unsupervised embedding of hierarchical structures with variational autoencoders, highlighting how hyperbolic geometry enhances separability of nested clusters. Applications of hyperbolic contrastive learning further demonstrate the efficiency of clustering in negatively curved spaces [19].

These advances motivate our proposed **HypeGBMS**, which integrates the density-seeking behavior of GBMS with the geometric priors of hyperbolic space. While GBMS provides smooth convergence to cluster modes in Euclidean settings, it fails to capture hierarchical structures. By embedding data into the Poincaré ball and redefining the update step through Möbius weighted means, HypeGBMS ensures that cluster assignments remain consistent with the geometry of the Poincaré ball. In doing so, our approach unifies density-based clustering with modern hyperbolic representation learning, addressing the limitations of classical mean-shift algorithms in hierarchical domains.

3 Preliminaries

We outline here the essential mathematical foundations of hyperbolic geometry relevant to this study. For a more comprehensive and rigorous exposition, we refer to the classical treatments in [20] and [21].

3.1 Hyperbolic space

A Hyperbolic space, denoted by \mathbb{H}^n , is a non-Euclidean space of dimension n , defined as a simply connected Riemannian manifold with constant sectional curvature -1 . The Killing–Hopf theorem [22] establishes that any two such spaces are isometric, implying that all realizations of \mathbb{H}^n are equivalent up to isometry.

1. **Poincaré Disc Model:** The Poincaré disc provides a representation of hyperbolic space in which all points lie within the open unit ball in \mathbb{R}^n . In this model, geodesics correspond either to Euclidean diameters of the disc or to circular arcs orthogonal to the boundary. For any two points \mathbf{X} and \mathbf{Y} satisfying $\|\mathbf{X}\|, \|\mathbf{Y}\| < 1$, the hyperbolic distance is given by:

$$d(\mathbf{X}, \mathbf{Y}) := \cosh^{-1} \left(1 + \frac{2\|\mathbf{X} - \mathbf{Y}\|^2}{(1 - \|\mathbf{X}\|^2)(1 - \|\mathbf{Y}\|^2)} \right). \quad (1)$$

2. **Hyperboloid Model:** The Hyperboloid model is also referred to as the Minkowski or Lorentz model. This formulation represents hyperbolic space as the forward sheet S^+ of a two-sheeted hyperboloid embedded in $(n + 1)$ -dimensional Minkowski space. For points $\mathbf{X} = (x_0, x_1, \dots, x_n)$ and $\mathbf{Y} = (y_0, y_1, \dots, y_n)$ lying on S^+ , the hyperbolic distance is defined as:

$$d(\mathbf{X}, \mathbf{Y}) := \cosh^{-1} (-M(\mathbf{X}, \mathbf{Y})), \quad (2)$$

where M denotes the Minkowski inner product, defined by:

$$\begin{aligned} M((x_0, x_1, \dots, x_n), (y_0, y_1, \dots, y_n)) \\ = -x_0y_0 + \sum_{i=1}^n x_iy_i. \end{aligned}$$

3.2 Gyrovector Spaces

The Gyrovector space framework offers a sophisticated algebraic structure suited for hyperbolic geometry, playing a role comparable to that of vector spaces in Euclidean geometry [23]. We define

$$\mathbb{D}_c^p := \{\mathbf{v} \in \mathbb{R}^p \mid -c\|\mathbf{v}\|^2 < 1\},$$

for curvature parameter $c < 0$. In the special case $c = 0$, this reduces to the Euclidean space \mathbb{R}^p . When $c < 0$, \mathbb{D}_c^p corresponds to an open ball with radius $1/\sqrt{-c}$, and choosing $c = -1$ recovers the unit ball \mathbb{D}^p .

The Poincaré Disc Model is especially advantageous computationally, as most of its geometric operations admit closed-form expressions. In this setting, we briefly introduce Möbius gyrovector addition and Möbius scalar multiplication. Since isometries preserve the intrinsic geometric structure of hyperbolic spaces, the underlying additive and multiplicative algebraic frameworks remain invariant under model transitions and may therefore be transported isomorphically across distinct representations of hyperbolic geometry without altering their essential nature [24]. To demonstrate this, we establish an explicit isometric correspondence between the Poincaré Disc Model and the hyperboloid model.

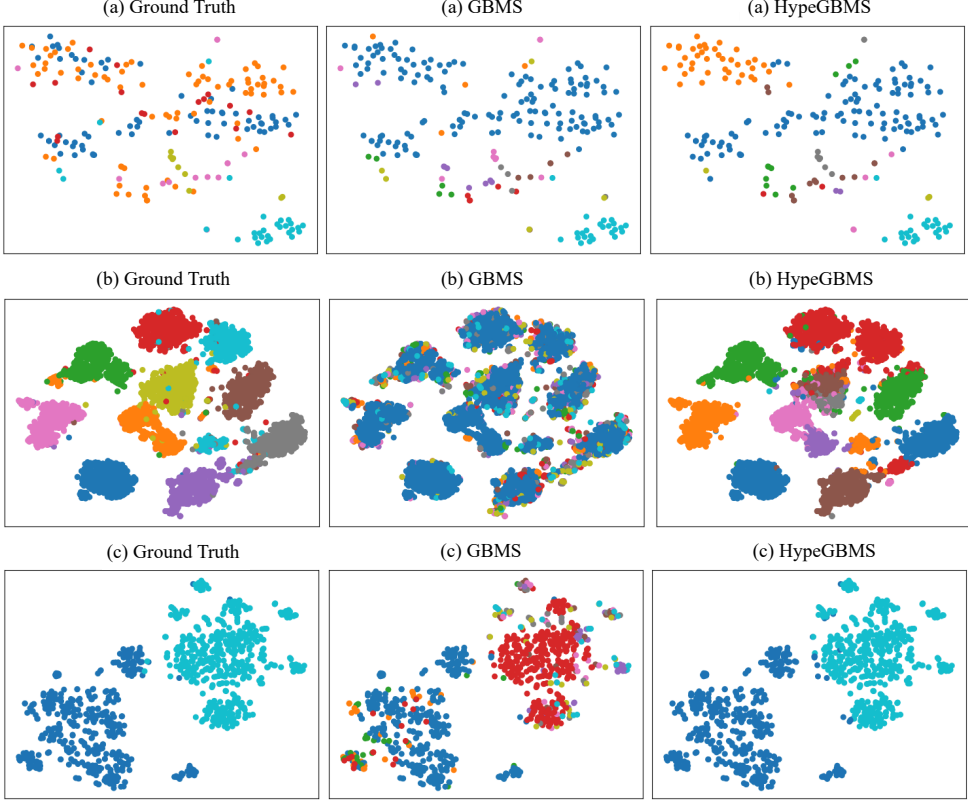


Fig. 1: The t-SNE Visualisation of real datasets (a) Glass, (b) ORHD, (c) Phishing URL, respectively for GBMS and HypeGBMS (ours) clustering methods.

Let $\mathbb{D}^n = \{x \in \mathbb{R}^n : \|x\| < 1\}$ denote the Poincaré Disc model. The corresponding hyperboloid model is given by

$$\mathbb{H}^n = \{x \in \mathbb{R}^{n+1} : -x_0^2 + x_1^2 + \cdots + x_n^2 = -1, x_0 > 0\}.$$

An isometric map between these two models is defined by

$$\phi : \mathbb{D}^n \rightarrow \mathbb{H}^n, \quad x \mapsto \left(\frac{1 + \|x\|^2}{1 - \|x\|^2}, \frac{2x}{1 - \|x\|^2} \right).$$

This mapping preserves hyperbolic distance and induces the same Riemannian metric structure. Consequently, for the remainder of this work, we adopt the Poincaré Disc model as our primary representation [25, 26].

Möbius addition. The Möbius addition of \mathbf{v} and \mathbf{w} in \mathbb{D}_c^p is defined as :

$$\mathbf{v} \oplus_c \mathbf{w} := \frac{(1 - 2c\langle \mathbf{v}, \mathbf{w} \rangle - c\|\mathbf{w}\|^2) \mathbf{v} + (1 + c\|\mathbf{v}\|^2) \mathbf{w}}{1 - 2c\langle \mathbf{v}, \mathbf{w} \rangle + c^2\|\mathbf{v}\|^2\|\mathbf{w}\|^2}. \quad (3)$$

In particular, when $c = 0$, this conforms with the Euclidean addition of two vectors in \mathbb{R}^p . However, it satisfies $\mathbf{v} \oplus_c \mathbf{0} = \mathbf{0} \oplus_c \mathbf{v} = \mathbf{v}$. Moreover, for any $\mathbf{v}, \mathbf{w} \in \mathbb{D}_c^p$, we have $(-\mathbf{v}) \oplus_c \mathbf{v} = \mathbf{v} \oplus_c (-\mathbf{v}) = \mathbf{0}$ and $(-\mathbf{v}) \oplus_c (\mathbf{v} \oplus_c \mathbf{w}) = \mathbf{w}$.

Möbius scalar multiplication. For $c < 0$, the Möbius scalar multiplication of $\mathbf{v} \in \mathbb{D}_c^p \setminus \{\mathbf{0}\}$ by a real number $\lambda \in \mathbb{R}$ is defined as,

$$\lambda \otimes_c \mathbf{v} := (1/\sqrt{-c}) \tanh(\lambda \tanh^{-1}(\sqrt{-c}\|\mathbf{v}\|)) \frac{\mathbf{v}}{\|\mathbf{v}\|}. \quad (4)$$

and $\lambda \otimes_c \mathbf{0} := \mathbf{0}$. As the parameter c approaches zero, the expression reverts to conventional Euclidean scalar multiplication: $\lim_{c \rightarrow 0} \lambda \otimes_c \mathbf{v} = \lambda \mathbf{v}$.

The Hyperbolic Distance function on (\mathbb{D}_c^p, g^c) is given by,

$$d_{\mathbb{H}}(\mathbf{v}, \mathbf{w}) = (2/\sqrt{-c}) \tanh^{-1}(\sqrt{-c}\|\mathbf{v} \oplus_c \mathbf{w}\|).$$

Riemannian Log-Exp Map. Given two points $x, y \in \mathbb{D}_c^p$, the logarithmic map at x applied to y is denoted as:

$$\log_x(y) = \frac{2}{\lambda_x} \cdot \frac{\tanh^{-1}(\sqrt{-c} \cdot \| -x \oplus_c y \|)}{\| -x \oplus_c y \|} \cdot (-x \oplus_c y), \quad (5)$$

where $\lambda_x = \frac{2}{1 - \lambda_x \|x\|^2}$ and \oplus_c represents the Möbius gyrovector addition as Equation (3).

Given $x \in \mathbb{D}_c^p$, $v \in T_x(\mathbb{D}_c^p)$, the exponential map is defined as,

$$\exp_x(v) = x \oplus_c \left(\tanh\left(\frac{\lambda_x \cdot \sqrt{-c} \cdot \|v\|}{2}\right) \cdot \frac{v}{\sqrt{-c} \cdot \|v\|} \right). \quad (6)$$

As the parameter c approaches 0,

$$\lim_{c \rightarrow 0} \exp_x(v) = (x + v), \quad (7)$$

$$\lim_{c \rightarrow 0} \log_x(y) = (y - x), \quad (8)$$

which are the exponential and logarithmic maps in Euclidean space.

4 HypeGBMS: our proposed method

We discuss our proposed method HypeGBMS in detail in Algorithm 2. The updated steps in our algorithm are marked in blue.

Algorithm 1 Gaussian Blurring Mean-Shift (GBMS) Algorithm

- 1: **Input:** Dataset $\mathbf{X} \in \mathbb{R}^{N \times p}$, bandwidth parameter $\sigma > 0$, convergence threshold $\tau > 0$, maximum iteration T .
- 2: **Output:** Cluster assignments $C_1, C_2, C_3, \dots, C_K$.
- 3: **1. Initialize:**
 - 4: Set iteration counter $t \leftarrow 0$.
 - 5: Initialise points $\mathbf{x}_i^{(0)} = \mathbf{x}_i$ for $i = 1, \dots, N$.
- 6: **2. For** $t = 1$ to T :
 - 7: Compute pairwise squared Euclidean distances:
$$(d_{ij}^{(t)})^2 = \|\mathbf{x}_i^{(t)} - \mathbf{x}_j^{(t)}\|^2$$
 - 8: Compute the Gaussian kernel weights:
$$w_{ij}^{(t)} \leftarrow \exp\left(-\frac{(d_{ij}^{(t)})^2}{2\sigma^2}\right)$$
 - 9: Normalise the weights row-wise:
$$\bar{w}_{ij}^{(t)} = \frac{w_{ij}^{(t)}}{\sum_k w_{ik}^{(t)}}$$
 - 10: Update each data point using weighted mean:
$$\mathbf{x}_i^{(t+1)} = \sum_{j=1}^N \bar{w}_{ij}^{(t)} \mathbf{x}_j^{(t)}$$
 - 11: Compute average movement across all points:
$$\Delta^{(t)} = \frac{1}{N} \sum_{i=1}^N \|\mathbf{x}_i^{(t+1)} - \mathbf{x}_i^{(t)}\|$$
 - 12: Check Convergence:
 - 13: If $\Delta^{(t)} < \tau$, **break**.
- 14: **3. Cluster Assignment:**
 - 15: Construct adjacency matrix from final $\mathbf{X}^{(T)}$.
 - 16: Identify connected components as clusters.

Step 1: Projecting onto the Poincaré Ball. We consider the dataset $X \in \mathbb{R}^{N \times p}$. We embed the data set into the hyperbolic space, here the Poincaré Ball model of radius $\frac{1}{\sqrt{-c}}, c < 0$ using the Riemannian Exponential map mentioned in Equation (6). We obtain $\tilde{\mathbf{X}} = \{\tilde{\mathbf{x}}_1, \tilde{\mathbf{x}}_2, \dots, \tilde{\mathbf{x}}_N\} \in \mathbb{D}_c^p$, where $\mathbb{D}_c^p := \{\mathbf{x} \in \mathbb{R}^p \mid -c\|\mathbf{x}\|^2 < 1\}$.

Step 2: Iterative Update Loop (for $t = 1$ to T)

Computing Pairwise Squared Hyperbolic Distances: We compute the pairwise squared hyperbolic distances as,

$$(d_{ij}^{(t)})^2 = d_{\mathbb{H}}^2(\tilde{\mathbf{x}}_i^{(t)}, \tilde{\mathbf{x}}_j^{(t)}) \quad (9)$$

Algorithm 2 Hyperbolic Gaussian Blurring Mean-Shift (HypeGBMS) Algorithm

- 1: **Input:** Dataset $\mathbf{X} \in \mathbb{R}^{N \times p}$, bandwidth parameter $\sigma > 0$, convergence threshold $\varepsilon > 0$, minimum cluster separation $\delta > 0$, maximum iteration T , curvature parameter $c < 0$.
- 2: **Output:** Cluster assignments $C_1, C_2, C_3, \dots, C_K$.
- 3: **1. Initialize:**
 - 4: Set iteration counter $t \leftarrow 0$.
 - 5: $\mathbf{X} \leftarrow \text{project onto Poincaré ball}(\mathbf{X}, c)$
- 6: **2. For** $t = 1$ to T :
 - 7: Compute pairwise squared hyperbolic distances:
$$(d_{ij}^{(t)})^2 = d_{\mathbb{H}}^2(\tilde{\mathbf{x}}_i^{(t)}, \tilde{\mathbf{x}}_j^{(t)})$$
 - 8: Compute the Gaussian kernel weights
$$w_{ij}^{(t)} \leftarrow \exp\left(-\frac{(d_{ij}^{(t)})^2}{2\sigma^2}\right)$$
 - 9: Normalise the weights row-wise:
$$\bar{w}_{ij}^{(t)} = \frac{w_{ij}^{(t)}}{\sum_k w_{ik}^{(t)}}$$
 - 10: Compute Möbius Weighted Mean:
$$\tilde{\mathbf{x}}_i^{(t+1)} = \bigoplus_{j=1}^N \bar{w}_{ij}^{(t)} \otimes_c \tilde{\mathbf{x}}_j^{(t)}$$
 - 11: Compute average movement:
$$\Delta^{(t)} = \frac{1}{N} \sum_{i=1}^N \left\| \log_{\tilde{\mathbf{x}}_i^{(t)}} (\tilde{\mathbf{x}}_i^{(t+1)}) \right\|$$
 - 12: Check Convergence
 - 13: If $\Delta^{(t)} < \varepsilon$, **break**.
- 14: **3. Cluster Assignment:**
 - 15: Construct adjacency matrix from final $\tilde{\mathbf{X}}^{(T)}$.
 - 16: Identify connected components as clusters.

where the poincaré ball distance is given by:

$$d_{\mathbb{H}}(\mathbf{x}, \mathbf{y}) = \frac{2}{\sqrt{-c}} \tanh^{-1} \left(\sqrt{-c} \left\| \mathbf{x} \oplus_c \mathbf{y} \right\| \right) \quad (10)$$

Computing Gaussian Kernel Weights: We construct the weight matrix, $\mathbf{W} = (w_{ij})_{N \times N}$ where the entries are defined as,

$$w_{ij}^{(t)} = \exp\left(-\frac{(d_{ij}^{(t)})^2}{2\sigma^2}\right), \quad (11)$$

where, d_{ij} are defined as Equation (9), σ is the bandwidth parameter.

Normalize the weights Row-wise: Now, we normalize the weight matrix, W as

$$\bar{w}_{ij}^{(t)} = \frac{w_{ij}^{(t)}}{\sum_{k=1}^n w_{ik}^{(t)}} \quad (12)$$

Computing Möbius Weighted Mean for each point: We define the möbius weighted mean as, $\bigoplus_{j=1}^N \bar{w}_{ij}^{(t)} \otimes_c \tilde{\mathbf{x}}_j^{(t)}$, where \bigoplus_j is Möbius addition defined as 3 and \otimes_c is the Möbius scalar multiplication as 4.

$$\tilde{\mathbf{x}}_i^{(t+1)} \leftarrow \text{MöbiusWeightedMean}(\{\tilde{\mathbf{x}}_j^{(t)}\}, \{\bar{w}_{ij}^{(t)}\}, c) \quad (13)$$

Computing Average Movement: We define the average movement as

$$\Delta^{(t)} = \frac{1}{N} \sum_{i=1}^N \left\| \log_{\tilde{\mathbf{x}}_i^{(t)}} (\tilde{\mathbf{x}}_i^{(t+1)}) \right\|, \quad (14)$$

where the logarithm map is defined as 5.

Checking Convergence:

If $\Delta^{(t)} < \varepsilon$ or $t = T$, then we stop the iteration.

Step 3: Cluster Assignment. Let $\tilde{\mathbf{X}}^{(T)} = \{\tilde{\mathbf{x}}_1^{(T)}, \dots, \tilde{\mathbf{x}}_N^{(T)}\}$. We construct an adjacency matrix $A \in \{0, 1\}^{N \times N}$ defined by

$$A_{ij} = \begin{cases} 1, & \text{if } d_{\mathbb{H}}(\tilde{\mathbf{x}}_i^{(T)}, \tilde{\mathbf{x}}_j^{(T)}) \leq \delta, \\ 0, & \text{otherwise,} \end{cases}$$

where $d_{\mathbb{H}}(\cdot, \cdot)$ is the hyperbolic distance and $\delta > 0$ is a threshold defined as minimum cluster separation. Interpreting A as the adjacency matrix of an undirected graph $G = (V, E)$ with vertex set $V = \{1, \dots, N\}$ and edges $(i, j) \in E$ whenever $A_{ij} = 1$, the final clustering is obtained by extracting its connected components. Thus, the resulting cluster set is $\mathbf{C} = \{C_1, \dots, C_K\}$, where each C_k corresponds to one connected component and K denotes the number of such components.

5 Stopping Criteria for HypeGBMS

The HypeGBMS algorithm terminates when the average movement drops below a certain tolerance limit, $\varepsilon = 10^{-5}$, that is:

$$\Delta^{(t)} < \varepsilon,$$

where $\Delta^{(t)}$ is defined as Equation (14). In iteration t , the update $\{\Delta_i^{(t)} = \|\log_{\tilde{\mathbf{x}}_i^{(t)}} \tilde{\mathbf{x}}_i^{(t+1)}\|\}$ for $i = 1, 2, \dots, N$ takes at most K different values (for K clusters) and a histogram of $\{\Delta_i^{(t)}\}_{i=1}^N$ has K or fewer nonempty bins. In summary, our stopping criterion is:

$$\Delta^{(t)} < \varepsilon \quad \text{OR} \quad |H^{(t+1)} - H^{(t)}| < \gamma, \quad (15)$$

where the Shannon entropy is given by:

$$H^{(t)} = - \sum_{k=1}^S p_k \log p_k,$$

where p_k is the normalized bin counts such that $\sum_{k=1}^S p_k = 1$. The number of bins S should be larger than the number of clusters but smaller than N ; we use $S = 0.9N$. Checking this criterion requires the time complexity of $\mathcal{O}(N)$.

6 Computational Complexity Analysis of HypeGBMS

In this section, we will present the step-by-step complexity analysis of our proposed method, HypeGBMS.

Step 1: Projecting onto the Poincaré Ball. We consider the dataset $X \in \mathbb{R}^{N \times p}$ and project onto the Poincaré Ball. This step requires the time complexity of $\mathcal{O}(N \times p)$.

Step 2: Iteration Loop ($t = 1$ to T)

Computing Pairwise Squared Hyperbolic Distances. We compute the hyperbolic distance between every pair of points by Equation (9). Each hyperbolic distance computation involves dot products in the p -dimensional space that requires the time complexity of $\mathcal{O}(p)$. So, for a total of N^2 pairs, the time complexity is $\mathcal{O}(N^2 \times p)$.

Computing Gaussian Kernel Weights. We apply the exponential function to N^2 distance values. The time complexity for this step is $\mathcal{O}(N^2)$. For each of N rows: sum N weights, then dividing N weights to normalise requires the time complexity of $\mathcal{O}(N^2)$.

Computing Möbius Weighted Mean for each point. Each point is updated using the weighted mean of N points. Each Möbius weighted mean computation in the Poincaré disc model involves Möbius addition and Möbius scalar multiplication, which require the time complexity of $\mathcal{O}(N \times p)$ for each point. The total complexity for this step becomes $\mathcal{O}(N^2 \times p)$.

Computing the Average Movement. We compute the logarithmic map for N points, which requires $N \times \mathcal{O}(p)$. So, the time complexity for this step in each iteration becomes $\mathcal{O}(N \times p)$.

Step 3: Cluster Assignment. After convergence, from the final $\tilde{\mathbf{X}}^{(T)}$, computing pairwise distances again and thresholding yields $\mathcal{O}(N^2 \times p)$. Interpreting the adjacency matrix as a dense graph with N nodes and $\mathcal{O}(N^2)$ edges costs $\mathcal{O}(N^2)$. Thus, the cost in Step 3 is $\mathcal{O}(N^2 \times p)$.

Therefore, the overall time complexity for our proposed algorithm is $\mathcal{O}(T \times N^2 \times p)$.

Remark on Scalable Approximations. Although the worst-case computational cost of HypeGBMS is $\mathcal{O}(TN^2p)$ due to the pairwise hyperbolic distance evaluations, this quadratic scaling becomes prohibitive for large-scale datasets. Several well-established approximation techniques from large-scale kernel methods

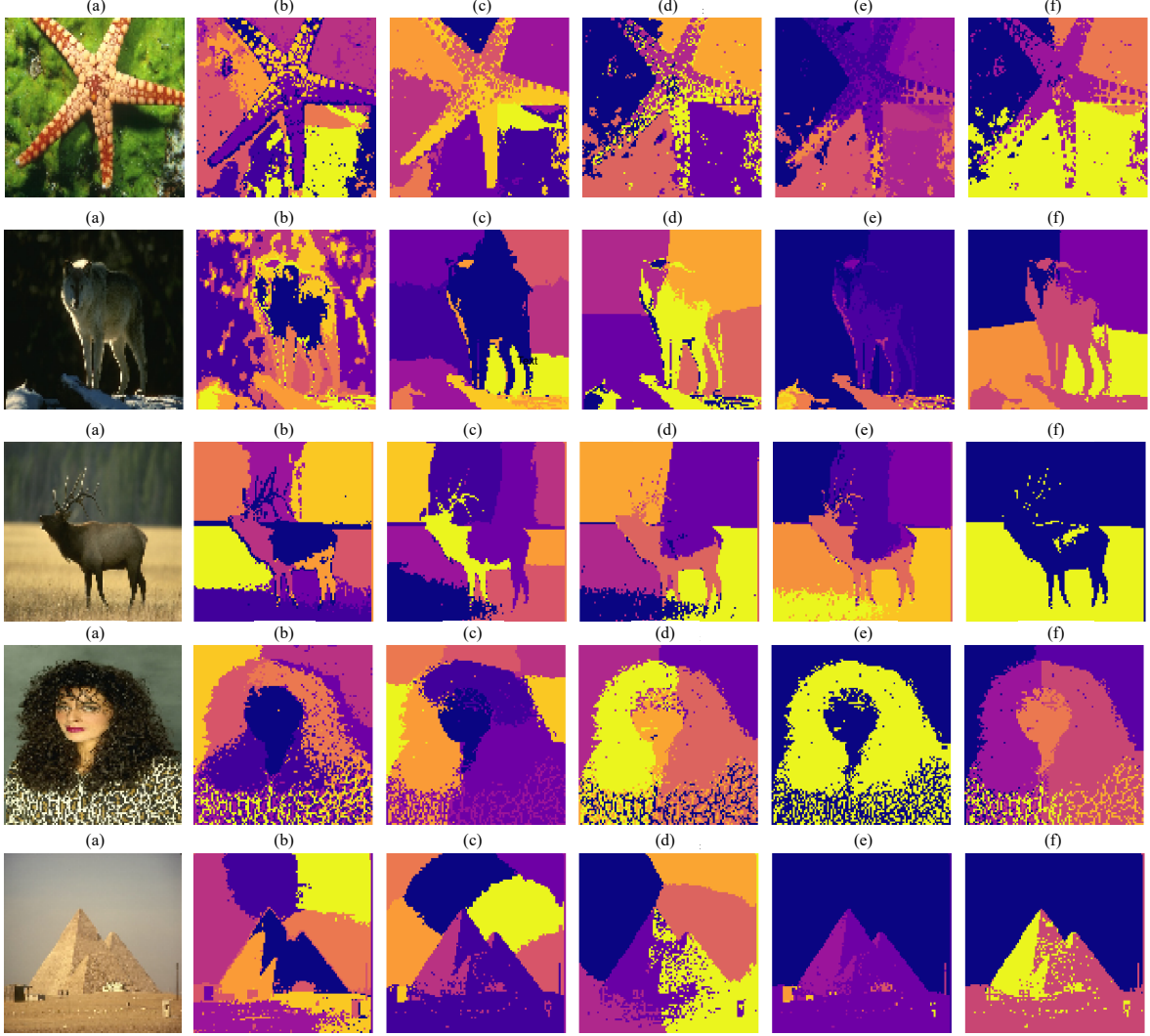


Fig. 2: Qualitative results on the BSDS500 dataset (a) Image, (b) GMS, (c) Gridshift, (d) QuickMeanshift, (e) GBMS, (f) HypeGBMS(ours).

and nearest-neighbor search can be introduced to reduce the effective cost. For example, tree-based search structures such as KD-trees and ball trees [27, 28] and their modern descendants (e.g., FLANN [29]) provide sublinear approximate nearest-neighbor queries in general metric spaces, including negatively curved ones. Similarly, kernel approximation schemes such as the Nyström method [30] and random feature expansions [31] reduce the effective kernel complexity from $\mathcal{O}(N^2)$ to near-linear in N . These ideas parallel acceleration strategies used in fast density-based clustering methods such as QuickShift++ [32]. Adapting such approximation frameworks to the hyperbolic setting offers a promising direction for developing scalable variants of HypeGBMS.

7 Convergence Analysis of HypeGBMS

This section provides a rigorous convergence analysis of the proposed HypeGBMS algorithm on the Poincaré ball model (\mathbb{D}_c^p, g_c) of constant curvature $c < 0$. Our analysis explicitly distinguishes the Möbius weighted mean used in Algorithm 2 from the Riemannian Fréchet mean required for standard convergence proofs and establishes curvature–radius dependent error bounds ensuring asymptotic convergence.

Let (\mathbb{D}_c^p, g_c) be the p -dimensional Poincaré ball with sectional curvature $c = -\kappa < 0$ and hyperbolic distance $d_{\mathbb{H}}$. The Möbius weighted mean (\bar{x}_M) used in Algorithm 2 is defined as Equation (13). The weighted Riemannian Fréchet mean is defined as:

$$\bar{x}_F = \arg \min_{z \in \mathbb{D}_c^p} F(z) := \arg \min_{z \in \mathbb{D}_c^p} \sum_{j=1}^N w_{ij} d_{\mathbb{H}}^2(z, x_j). \quad (16)$$

Proposition 1 Let $\{x_j\}_{j=1}^N \subset \mathbb{D}_c^p$ lie within a geodesic ball $B_{\mathbb{H}}(x_0, r)$ of radius $r < 1$ and curvature magnitude $\kappa = -c > 0$. Then there exists a constant $C_p > 0$, depending only on dimension p , such that

$$d_{\mathbb{H}}(\bar{x}_M, \bar{x}_F) \leq C_p \kappa r^3. \quad (17)$$

Moreover, $\bar{x}_M, \bar{x}_F \in B_{\mathbb{H}}(x_0, r)$.

The proof is shown in the Appendix.

Remark. This proposition suggests that when all points lie in a sufficiently small ball, the Möbius weighted mean (\bar{x}_M) is a first-order (in the radius r) approximation $[\cdot : r = \frac{1}{\sqrt{\kappa}}]$ of the Fréchet mean (\bar{x}_F) . As in $r \rightarrow 0$, the two notions of mean converge, and both reduce to the Euclidean barycenter in the tangent space.

7.1 Boundedness of Iterates

Lemma 1 (Iterates remain in a geodesically convex subset) Suppose the initial points $\{\tilde{x}_i^{(0)}\}$ lie in a compact, geodesically convex subset $\mathcal{U} \subset \mathbb{D}_c^p$ of radius $r < 1$. Then for all $t \geq 0$,

$$\tilde{x}_i^{(t)} \in \mathcal{U}, \quad d_{\mathbb{H}}(\tilde{x}_i^{(t+1)}, \tilde{x}_k^{(t+1)}) \leq (1 + \alpha) d_{\mathbb{H}}(\tilde{x}_i^{(t)}, \tilde{x}_k^{(t)}),$$

where $\alpha = C_p \kappa r^2$.

Proof Let $T_i^{(t)} : \mathbb{D}_c^p \rightarrow \mathbb{D}_c^p$ be the update map such that

$$T_i^{(t)}(x) = \text{MöbiusWeightedMean}(\{\tilde{x}_j^{(t)}\}, \{w_{ij}^{(t)}\}, c).$$

Let $\Phi_i^{(t)} : \mathbb{D}_c^p \rightarrow \mathbb{D}_c^p$ be the update map such that

$$\Phi_i^{(t)}(x) = \arg \min_{x \in \mathbb{D}_c^p} \sum_{j=1}^N w_{ij} d_{\mathbb{H}}^2(x, \tilde{x}_j^{(t)})$$

From Proposition 1, $T_i^{(t)}$ is an $\mathcal{O}(\kappa r^3)$ -approximation of the exact Fréchet mean map $\Phi_i^{(t)}$. Weighted Riemannian barycentric maps are non-expansive in any CAT(0) space (including the Poincaré ball), thus: $d_{\mathbb{H}}(\Phi_i^{(t)}(x), \Phi_k^{(t)}(y)) \leq d_{\mathbb{H}}(x, y)$ [33]. By the triangle inequality,

$$\begin{aligned} d_{\mathbb{H}}(T_i^{(t)}(x), T_k^{(t)}(y)) &\leq d_{\mathbb{H}}(T_i^{(t)}(x), \Phi_i^{(t)}(x)) + d_{\mathbb{H}}(\Phi_i^{(t)}(x), \Phi_k^{(t)}(y)) + d_{\mathbb{H}}(T_k^{(t)}(y), \Phi_k^{(t)}(y)) \\ &\leq (1 + \mathcal{O}(\kappa r^2)) d_{\mathbb{H}}(x, y), \end{aligned}$$

giving the required $(1 + \alpha)$ factor, where $\alpha = C_p \kappa r^2$. Compactness of \mathcal{U} ensures iterates remain in \mathcal{U} . \square

7.2 Convergence of HypeGBMS

Theorem 2 (Convergence of HypeGBMS) Let $\{\tilde{x}_i^{(t)}\}_{t \geq 0}$ denote the sequence generated by Algorithm 2. Assume all iterates lie in a convex ball $\mathcal{U} \subset \mathbb{D}_c^p$ of radius $r < 1$ and curvature magnitude $\kappa = -c$. Then:

1. The sequence $\hat{f}(\tilde{x}_i^{(t)})$ with

$$\hat{f}(x) = \frac{1}{N} \sum_{j=1}^N \exp\left(-\frac{d_{\mathbb{H}}^2(x, \tilde{x}_j)}{2\sigma^2}\right)$$

is monotone non-decreasing up to additive errors $\mathcal{O}(\kappa r^3)$ and convergent.

2. Each $\tilde{x}_i^{(t)}$ converges to a point \tilde{x}_i^* satisfying $\|\nabla_{\mathbb{H}} \hat{f}(\tilde{x}_i^*)\| \leq C_p \kappa r^3$.

In the limit $\kappa r^3 \rightarrow 0$, \tilde{x}_i^* is an exact stationary point of \hat{f} .

Proof By Lemma 1, iterates remain in a compact convex set \mathcal{U} where curvature, metric, and derivatives of \hat{f} are bounded. Let $\Phi_i^{(t)}$ be the exact Fréchet mean update. Then $\Phi_i^{(t)}$ performs a Riemannian gradient ascent on \hat{f} with step size $\eta = 1/\sigma^2$ [33], implying $\hat{f}(\Phi_i^{(t)}(\tilde{x}_i^{(t)})) - \hat{f}(\tilde{x}_i^{(t)}) \geq c_1 \|\nabla_{\mathbb{H}} \hat{f}(\tilde{x}_i^{(t)})\|^2$ for some $c_1 > 0$, where the Riemannian gradient of \hat{f} is

$$\nabla_{\mathbb{H}} \hat{f}(\mathbf{x}) = \frac{1}{N\sigma^2} \sum_{j=1}^N K_{\sigma}(\mathbf{x}, \tilde{x}_j) \log_{\mathbf{x}}(\tilde{x}_j), \quad (18)$$

where $K_{\sigma}(\mathbf{x}, \tilde{x}_j) = \exp(-d_{\mathbb{H}}^2(\mathbf{x}, \tilde{x}_j)/(2\sigma^2))$ and $\log_{\mathbf{x}}(\cdot)$ is the Riemannian logarithmic map as 5. Using Proposition 1, the Möbius update $T_i^{(t)}$ satisfies $d_{\mathbb{H}}(T_i^{(t)}(\tilde{x}_i^{(t)}), \Phi_i^{(t)}(\tilde{x}_i^{(t)})) \leq C_p \kappa r^3$, so by Lipschitz continuity of \hat{f} we get

$$\hat{f}(T_i^{(t)}(\tilde{x}_i^{(t)})) \geq \hat{f}(\Phi_i^{(t)}(\tilde{x}_i^{(t)})) - C_p \kappa r^3 \geq \hat{f}(\tilde{x}_i^{(t)}) + c_1 \|\nabla_{\mathbb{H}} \hat{f}(\tilde{x}_i^{(t)})\|^2 - C_p \kappa r^3. \quad (19)$$

Hence $\{\hat{f}(\tilde{\mathbf{x}}_i^{(t)})\}$ is a monotone non-decreasing sequence bounded above (since $0 < \hat{f}(\mathbf{x}) \leq 1$). Hence, it converges by the Monotone convergence theorem [34]. Summing the inequality (19) over t yields $\sum_t \|\nabla_{\mathbb{H}} \hat{f}(\tilde{\mathbf{x}}_i^{(t)})\|^2 < \infty$, implying $\|\nabla_{\mathbb{H}} \hat{f}(\tilde{\mathbf{x}}_i^{(t)})\| \rightarrow 0$ up to $\mathcal{O}(\kappa r^3)$, so each limit point $\tilde{\mathbf{x}}_i^*$ satisfies the claimed condition. \square

The above results establish that the Möbius update constitutes an *inexact Riemannian gradient ascent* whose inexactness vanishes with both curvature magnitude and local cluster radius. Therefore, HypeGBMS inherits the convergence behavior of classical GBMS in the small-curvature regime and converges to approximate Fréchet stationary points under bounded curvature.

8 Statistical Consistency of HypeGBMS

We now establish a consistency result for the cluster centroids obtained by the proposed HypeGBMS method. Let (\mathbb{D}_c^p, g_c) denote the Poincaré ball model of hyperbolic space with curvature $c < 0$ and metric tensor g . Let $d_{\mathbb{H}}(\cdot, \cdot)$ be the corresponding hyperbolic distance as mentioned in Equation (10). Let $X_1, \dots, X_N \stackrel{iid}{\sim} P$ with density f supported on a compact subset of \mathbb{D}_c^p . For bandwidth $\sigma > 0$, the kernel is

$$K_\sigma(x, y) = \exp\left(-\frac{d_{\mathbb{H}}^2(x, y)}{2\sigma^2}\right), \quad (20)$$

and the empirical kernel density estimator (KDE) is :

$$\hat{f}_\sigma(x) = \frac{1}{N} \sum_{i=1}^N K_\sigma(x, X_i).$$

The population smoothed density is

$$f_\sigma(x) = \int_{\mathbb{D}_c^p} K_\sigma(x, y) f(y) d\text{vol}_{\mathbb{H}}(y).$$

Modes of f_σ are :

$$\mathcal{M}_\sigma = \{m_1, \dots, m_K\}, \quad m_j = \arg \max_{x \in U_j} f_\sigma(x),$$

where U_j are disjoint neighborhoods of each mode. The empirical analogues $\hat{\mathcal{M}}_\sigma$ are the stationary points obtained by HypeGBMS.

Lemma 2 Suppose f is continuous and bounded, and the kernel K_σ is smooth in x . Then as $N \rightarrow \infty$,

$$\sup_{x \in \mathbb{D}_c^p} |\hat{f}_\sigma(x) - f_\sigma(x)| \xrightarrow{a.s.} 0,$$

and

$$\sup_{x \in \mathbb{D}_c^p} \|\nabla_{\mathbb{H}} \hat{f}_\sigma(x) - \nabla_{\mathbb{H}} f_\sigma(x)\| \xrightarrow{a.s.} 0.$$

Proof Since f is supported on a compact subset of \mathbb{D}_c^p , there exists a compact geodesically convex set $\mathcal{U} \subset \mathbb{D}_c^p$ such that $\text{supp}(f) \subset \mathcal{U}$. It suffices to prove the uniform convergence on \mathcal{U} :

$$\begin{aligned} \sup_{x \in \mathcal{U}} |\hat{f}_\sigma(x) - f_\sigma(x)| &\xrightarrow{a.s.} 0, \\ \sup_{x \in \mathcal{U}} \|\nabla_{\mathbb{H}} \hat{f}_\sigma(x) - \nabla_{\mathbb{H}} f_\sigma(x)\| &\xrightarrow{a.s.} 0, \end{aligned}$$

since outside \mathcal{U} the density f vanishes and both f_σ and \hat{f}_σ are determined by their values on \mathcal{U} . For each fixed $x \in \mathcal{U}$, define the function

$$\varphi_x(y) := K_\sigma(x, y) = \exp\left(-\frac{d_{\mathbb{H}}^2(x, y)}{2\sigma^2}\right), \quad y \in \mathbb{D}_c^p.$$

Then

$$\hat{f}_\sigma(x) = \frac{1}{N} \sum_{i=1}^N \varphi_x(X_i), \quad f_\sigma(x) = \mathbb{E}[\varphi_x(X_1)].$$

Because K_σ is continuous and $d_{\mathbb{H}}(x, y) \geq 0$, there exists a finite constant $M > 0$ such that $|\varphi_x(y)| \leq M$ for all $x \in \mathcal{U}$ and all $y \in \mathbb{D}_c^p$. For each fixed x , the random variables $\{\varphi_x(X_i)\}_{i \geq 1}$ are i.i.d. with $\mathbb{E}|\varphi_x(X_1)| < \infty$, so by the strong law of large numbers,

$$\frac{1}{N} \sum_{i=1}^N \varphi_x(X_i) \xrightarrow{a.s.} \mathbb{E}[\varphi_x(X_1)] = f_\sigma(x),$$



Fig. 3: Qualitative results on the PASCAL VOC 2012 dataset (a) Image, (b) GMS, (c) Gridshift, (d) QuickMeanshift, (e) GBMS, (f) HypeGBMS(ours).

Thus, for every fixed x , pointwise almost sure convergence holds. We now upgrade this to uniform convergence over $x \in \mathcal{U}$ using compactness and equicontinuity.

Since K_σ is smooth in x by assumption, and $(\mathcal{U} \times \mathcal{U})$ is compact, the Riemannian gradient of K_σ with respect to the first argument is uniformly bounded: there exists $L > 0$ such that,

$$\sup_{x,y \in \mathcal{U}} \|\nabla_{\mathbb{H}} K_\sigma(x,y)\| \leq L < \infty.$$

By the mean value inequality on Riemannian manifold, this implies that for all $x, x' \in \mathcal{U}$ and all $y \in \mathcal{U}$,

$$|K_\sigma(x,y) - K_\sigma(x',y)| \leq L d_{\mathbb{H}}(x,x'). \quad (21)$$

In particular, the family $\{\varphi_x : x \in \mathcal{U}\}$ is equicontinuous in x (uniformly in y). Since \mathcal{U} is compact, for every $\delta > 0$ there exists a finite δ -net $\{x_1, \dots, x_m\} \subset \mathcal{U}$ such that for every $x \in \mathcal{U}$ there is $k \in \{1, \dots, m\}$ with $d_{\mathbb{H}}(x, x_k) \leq \delta$. Fix $\varepsilon > 0$. Choose $\delta > 0$ such that

$$L \delta < \varepsilon/4.$$

Let $\{x_1, \dots, x_m\}$ be a finite δ -net of \mathcal{U} . For each $k \in \{1, \dots, m\}$, the strong law of large numbers implies

$$\hat{f}_\sigma(x_k) = \frac{1}{N} \sum_{i=1}^N K_\sigma(x_k, X_i) \xrightarrow{a.s.} f_\sigma(x_k),$$

as $N \rightarrow \infty$. Since $m < \infty$, by union bound [35] and the fact that a finite union of almost sure events is almost sure, we have

$$\max_{1 \leq k \leq m} |\hat{f}_\sigma(x_k) - f_\sigma(x_k)| \xrightarrow{a.s.} 0.$$

Thus, with probability 1, there exists N_0 such that for all $N \geq N_0$,

$$\max_{1 \leq k \leq m} |\hat{f}_\sigma(x_k) - f_\sigma(x_k)| < \varepsilon/2.$$

Now fix such an N and consider any $x \in \mathcal{U}$. Choose k such that $d_{\mathbb{H}}(x, x_k) \leq \delta$. Then

$$|\hat{f}_\sigma(x) - f_\sigma(x)| \leq |\hat{f}_\sigma(x) - \hat{f}_\sigma(x_k)| + |\hat{f}_\sigma(x_k) - f_\sigma(x_k)| + |f_\sigma(x_k) - f_\sigma(x)|.$$

We bound each term:

(i) Using (21),

$$|\hat{f}_\sigma(x) - \hat{f}_\sigma(x_k)| = \left| \frac{1}{N} \sum_{i=1}^N (K_\sigma(x, X_i) - K_\sigma(x_k, X_i)) \right|$$

$$\begin{aligned}
&\leq \frac{1}{N} \sum_{i=1}^N |K_\sigma(x, X_i) - K_\sigma(x_k, X_i)| \\
&\leq \frac{1}{N} \sum_{i=1}^N L d_{\mathbb{H}}(x, x_k) \leq L \delta < \varepsilon/4.
\end{aligned}$$

(ii) By the choice of $N \geq N_0$,

$$|\hat{f}_\sigma(x_k) - f_\sigma(x_k)| < \varepsilon/2.$$

(iii) Since K_σ and f are bounded and K_σ is Lipschitz in x as in (21), we obtain by the Dominated Convergence theorem [34],

$$\begin{aligned}
|f_\sigma(x) - f_\sigma(x_k)| &= \left| \int (K_\sigma(x, y) - K_\sigma(x_k, y)) f(y) d\text{vol}_{\mathbb{H}}(y) \right| \\
&\leq L \delta < \varepsilon/4.
\end{aligned}$$

Combining (i)–(iii), we obtain

$$|\hat{f}_\sigma(x) - f_\sigma(x)| < \varepsilon/4 + \varepsilon/2 + \varepsilon/4 = \varepsilon$$

for all $x \in \mathcal{U}$ and all $N \geq N_0$, almost surely. Hence

$$\sup_{x \in \mathcal{U}} |\hat{f}_\sigma(x) - f_\sigma(x)| \xrightarrow{a.s.} 0,$$

which proves the first claim.

The argument for the gradient is analogous. By a similar kind of argument, we can show that :

$$\sup_{x \in \mathcal{U}} \|\nabla_{\mathbb{H}} \hat{f}_\sigma(x) - \nabla_{\mathbb{H}} f_\sigma(x)\| \xrightarrow{a.s.} 0.$$

Since \mathcal{U} contains the support of f and is compact, the same suprema over \mathbb{D}_c^p coincide with the suprema over \mathcal{U} . This proves the lemma. \square

Lemma 3 Suppose m is a non-degenerate critical point of f_σ , i.e.

$$\nabla_{\mathbb{H}} f_\sigma(m) = 0, \quad \text{Hess}_{\mathbb{H}} f_\sigma(m) \text{ is nonsingular.}$$

Then for large N , there exists a unique critical point \hat{m}_N of \hat{f}_σ such that

$$d_{\mathbb{H}}(\hat{m}_N, m) \rightarrow 0 \quad a.s.$$

Proof By Lemma 2, the empirical gradient converges uniformly to the population gradient on compact subset \mathcal{U} :

$$\sup_{x \in \mathcal{U}} \|\nabla_{\mathbb{H}} \hat{f}_\sigma(x) - \nabla_{\mathbb{H}} f_\sigma(x)\| \xrightarrow[N \rightarrow \infty]{a.s.} 0.$$

In particular, this holds on a geodesic ball $B_{\mathbb{H}}(m, r)$ for $r > 0$ sufficiently small. Consider normal coordinates $\xi \in T_m \mathcal{M} \cong \mathbb{R}^p$ defined by $x = \exp_m(\xi)$, and mappings

$$\begin{aligned}
F(\xi) &:= \nabla_{\mathbb{H}} f_\sigma(\exp_m(\xi)), \\
\hat{F}_N(\xi) &:= \nabla_{\mathbb{H}} \hat{f}_\sigma(\exp_m(\xi)).
\end{aligned}$$

Since m is a nondegenerate critical point, we have $F(0) = 0$ and $DF(0) = \text{Hess}_{\mathbb{H}} f_\sigma(m)$, which is invertible by assumption. By continuity of the Hessian, there exists $r > 0$ such that $DF(\xi)$ remains invertible for all $\|\xi\| \leq r$. By the uniform convergence established above,

$$\sup_{\|\xi\| \leq r} \|\hat{F}_N(\xi) - F(\xi)\| \rightarrow 0 \quad a.s.,$$

so for sufficiently large N , the perturbation $(\hat{F}_N - F)$ is uniformly small on $B(0, r)$.

Since $DF(0)$ is invertible and $F(0) = 0$, there exists a unique zero of F inside $B(0, r)$, namely $\xi = 0$. The manifold version of the Implicit Function theorem [36]; for N sufficiently large, \hat{F}_N also admits a unique zero ξ_N inside $B(0, r)$ and that this zero depends continuously on the perturbation \hat{F}_N . Hence,

$$\xi_N \rightarrow 0 \quad \text{almost surely.}$$

Finally, since the Riemannian exponential map is a diffeomorphism in a normal neighborhood, the convergence $\xi_N \rightarrow 0$ implies

$$\hat{m}_N = \exp_m(\xi_N) \rightarrow \exp_m(0) = m \quad \text{almost surely,}$$

which completes the proof. \square

Theorem 3 Assume the following conditions hold:

1. f_σ is continuous and bounded with compact support in \mathbb{D}_c^p .

2. Each mode of f_σ is isolated and nondegenerate.

Then for each $m_j \in \mathcal{M}_\sigma$, there exists $\hat{m}_j \in \hat{\mathcal{M}}_\sigma$ such that

$$d_{\mathbb{H}}(\hat{m}_j, m_j) \xrightarrow{\mathbb{P}} 0.$$

that is convergence in probability.

Equivalently, in terms of the distance,

$$d_{\mathbb{H}}(\hat{\mathcal{M}}_\sigma, \mathcal{M}_\sigma) \xrightarrow{\mathbb{P}} 0.$$

Proof By assumption, f_σ has compact support in \mathbb{D}_c^p , say \mathcal{U} so let

$$\mathcal{U} := \text{supp}(f_\sigma),$$

which is compact by definition. By assumption, f_σ has finitely many isolated, nondegenerate modes

$$\mathcal{M}_\sigma = \{m_1, \dots, m_K\} \subset \mathcal{U}, \quad \nabla_{\mathbb{H}} f_\sigma(m_j) = 0, \quad \text{Hess}_{\mathbb{H}} f_\sigma(m_j) \text{ nonsingular.}$$

Since each mode is isolated, for each j we choose $r_j > 0$ sufficiently small so that the geodesic balls

$$B_j := B_{\mathbb{H}}(m_j, r_j)$$

satisfy:

- (i) The sets B_j are pairwise disjoint.
- (ii) m_j is the only critical point of f_σ in B_j .

Define the partition of the compact support:

$$\mathcal{B} := \bigcup_{j=1}^K (B_j \cap \mathcal{U}), \quad \mathcal{C} := \mathcal{U} \setminus \mathcal{B}.$$

Since \mathcal{U} is compact and \mathcal{B} is open in the subspace topology of \mathcal{U} , \mathcal{C} is closed in \mathcal{U} and therefore compact. As f_σ has no critical points in \mathcal{C} and $\nabla_{\mathbb{H}} f_\sigma$ is continuous, the minimum of its gradient norm on \mathcal{C} is strictly positive:

$$\inf_{x \in \mathcal{C}} \|\nabla_{\mathbb{H}} f_\sigma(x)\| := 2\delta > 0. \quad (22)$$

By Lemma 2, we have :

$$\sup_{x \in \mathcal{U}} \|\nabla_{\mathbb{H}} \hat{f}_\sigma(x) - \nabla_{\mathbb{H}} f_\sigma(x)\| \xrightarrow{a.s.} 0.$$

Therefore, for the δ from (22), there exists a random N_1 such that for all $N \geq N_1$,

$$\sup_{x \in \mathcal{U}} \|\nabla_{\mathbb{H}} \hat{f}_\sigma(x) - \nabla_{\mathbb{H}} f_\sigma(x)\| < \delta, \quad \text{a.s.} \quad (23)$$

For $x \in \mathcal{C}$ and $N \geq N_1$, using (22) and (23),

$$\|\nabla_{\mathbb{H}} \hat{f}_\sigma(x)\| \geq \|\nabla_{\mathbb{H}} f_\sigma(x)\| - \delta \geq 2\delta - \delta = \delta > 0.$$

Thus, for large N , \hat{f}_σ has no critical points in \mathcal{C} . Hence, all critical points of \hat{f}_σ inside \mathcal{U} lie in \mathcal{B} .

Fix $j \in \{1, \dots, K\}$. Since m_j is a nondegenerate critical point, Lemma 3 implies that for sufficiently large N , there exists a unique critical point \hat{m}_j of \hat{f}_σ inside $B_j \cap \mathcal{U}$. Thus,

$$d_{\mathbb{H}}(\hat{m}_j, m_j) \xrightarrow[N \rightarrow \infty]{\mathbb{P}} 0.$$

Now,

$$\begin{aligned} d_{\mathbb{H}}(\hat{\mathcal{M}}_\sigma, \mathcal{M}_\sigma) &:= \max \left\{ \sup_{\hat{m} \in \hat{\mathcal{M}}_\sigma} \inf_{m \in \mathcal{M}_\sigma} d_{\mathbb{H}}(\hat{m}, m), \right. \\ &\quad \left. \sup_{m \in \mathcal{M}_\sigma} \inf_{\hat{m} \in \hat{\mathcal{M}}_\sigma} d_{\mathbb{H}}(\hat{m}, m) \right\}. \end{aligned}$$

For sufficiently large N , each true mode m_j matches uniquely to \hat{m}_j , so

$$d_{\mathbb{H}}(\hat{\mathcal{M}}_\sigma, \mathcal{M}_\sigma) = \max_{1 \leq j \leq K} d_{\mathbb{H}}(\hat{m}_j, m_j).$$

Since $K < \infty$ and each term in the RHS converges in probability to 0, the maximum also converges in probability to 0:

$$d_{\mathbb{H}}(\hat{\mathcal{M}}_\sigma, \mathcal{M}_\sigma) \xrightarrow[N \rightarrow \infty]{\mathbb{P}} 0.$$

This completes the proof. \square

Theorem 4 If the bandwidth sequence satisfies

$$\sigma_N \rightarrow 0, \quad N\sigma_N^p \rightarrow \infty,$$

then the estimated centroids $\hat{\mathcal{M}}_{\sigma_N}$ converge in probability to the true modes of f .

Proof We now let the bandwidth depend on N , writing $\sigma_N \rightarrow 0$ with $N\sigma_N^p \rightarrow \infty$, and the KDE

$$\hat{f}_{\sigma_N}(x) = \frac{1}{N} \sum_{i=1}^n \exp\left(-\frac{d_{\mathbb{H}}^2(x, X_i)}{2\sigma_N^2}\right).$$

Let f be the true density with compact support $\mathcal{U} := \text{supp}(f)$, and for each $\sigma > 0$ define the population smoothed density

$$f_\sigma(x) = \int_{\mathbb{D}_c^p} K_\sigma(x, y) f(y) d\text{vol}_{\mathbb{H}}(y).$$

We assume that f has finitely many isolated, nondegenerate modes $\mathcal{M} = \{m_1, \dots, m_K\}$ in \mathcal{U} , so that each m_j satisfies

$$\nabla_{\mathbb{H}} f(m_j) = 0, \quad \text{Hess}_{\mathbb{H}} f(m_j) \text{ is nonsingular.}$$

The goal is to show that the empirical centroids $\hat{\mathcal{M}}_{\sigma_N}$ produced by HypeGBMS converge in probability to the true modes \mathcal{M} .

Consider the gradient error decomposition

$$\nabla_{\mathbb{H}} \hat{f}_{\sigma_N}(x) - \nabla_{\mathbb{H}} f(x) = (\nabla_{\mathbb{H}} \hat{f}_{\sigma_N}(x) - \nabla_{\mathbb{H}} f_{\sigma_N}(x)) + (\nabla_{\mathbb{H}} f_{\sigma_N}(x) - \nabla_{\mathbb{H}} f(x)).$$

We control each term uniformly over the compact support \mathcal{U} .

For each fixed N , Lemma 2 (applied with bandwidth σ_N) gives the *conditional* uniform convergence

$$\sup_{x \in \mathcal{U}} \|\nabla_{\mathbb{H}} \hat{f}_{\sigma_N}(x) - \nabla_{\mathbb{H}} f_{\sigma_N}(x)\| \xrightarrow[N \rightarrow \infty]{\mathbb{P}} 0$$

under the bandwidth condition $N\sigma_N^p \rightarrow \infty$. This follows from classical kernel density estimation theory on manifolds: the effective sample size in a ball of radius $O(\sigma_N)$ is $N\sigma_N^p$, and the variance term is of order $(N\sigma_N^p)^{-1/2}$, which vanishes under the assumed condition. Thus,

$$\sup_{x \in \mathcal{U}} \|\nabla_{\mathbb{H}} \hat{f}_{\sigma_N}(x) - \nabla_{\mathbb{H}} f_{\sigma_N}(x)\| \xrightarrow[N \rightarrow \infty]{\mathbb{P}} 0. \quad (24)$$

Because f is continuous with compact support and the kernel $K_\sigma(x, y) = \exp(-d_{\mathbb{H}}^2(x, y)/(2\sigma^2))$ is smooth and acts as an approximate identity as $\sigma \rightarrow 0$, standard arguments in Riemannian kernel smoothing [37] (using normal coordinates and Taylor expansion of f) imply that

$$\begin{aligned} \sup_{x \in \mathcal{U}} |f_{\sigma_N}(x) - f(x)| &\rightarrow 0, \\ \sup_{x \in \mathcal{U}} \|\nabla_{\mathbb{H}} f_{\sigma_N}(x) - \nabla_{\mathbb{H}} f(x)\| &\rightarrow 0 \end{aligned}$$

as $N \rightarrow \infty$ (since $\sigma_N \rightarrow 0$). Thus,

$$\sup_{x \in \mathcal{U}} \|\nabla_{\mathbb{H}} f_{\sigma_N}(x) - \nabla_{\mathbb{H}} f(x)\| \xrightarrow[N \rightarrow \infty]{\mathbb{P}} 0. \quad (25)$$

Combining (24) and (25) via the triangle inequality, we obtain

$$\sup_{x \in \mathcal{U}} \|\nabla_{\mathbb{H}} \hat{f}_{\sigma_N}(x) - \nabla_{\mathbb{H}} f(x)\| \leq \sup_{x \in \mathcal{U}} \|\nabla_{\mathbb{H}} \hat{f}_{\sigma_N}(x) - \nabla_{\mathbb{H}} f_{\sigma_N}(x)\| + \sup_{x \in \mathcal{U}} \|\nabla_{\mathbb{H}} f_{\sigma_N}(x) - \nabla_{\mathbb{H}} f(x)\|.$$

Thus, the empirical gradient field $\nabla_{\mathbb{H}} \hat{f}_{\sigma_N}$ converges uniformly in probability to the true gradient field $\nabla_{\mathbb{H}} f$ on the compact set \mathcal{U} :

$$\sup_{x \in \mathcal{U}} \|\nabla_{\mathbb{H}} \hat{f}_{\sigma_N}(x) - \nabla_{\mathbb{H}} f(x)\| \xrightarrow[N \rightarrow \infty]{\mathbb{P}} 0. \quad (26)$$

As in the proof of Theorem 3 (fixed bandwidth case), we exploit the nondegeneracy of the modes of f . For each mode $m_j \in \mathcal{M}$, choose a radius $r_j > 0$ such that the balls

$$B_j := B_{\mathbb{H}}(m_j, r_j)$$

are pairwise disjoint and each B_j contains no other critical point of f than m_j . Define

$$\mathcal{B} := \bigcup_{j=1}^K (B_j \cap \mathcal{U}), \quad \mathcal{C} := \mathcal{U} \setminus \mathcal{B}.$$

As before, \mathcal{C} is compact, contains no critical points of f , and by continuity of $\nabla_{\mathbb{H}} f$ there exists $\delta > 0$ such that

$$\inf_{x \in \mathcal{C}} \|\nabla_{\mathbb{H}} f(x)\| \geq 2\delta > 0. \quad (27)$$

By (26), for any $\varepsilon > 0$,

$$\mathbb{P}\left(\sup_{x \in \mathcal{U}} \|\nabla_{\mathbb{H}} \hat{f}_{\sigma_N}(x) - \nabla_{\mathbb{H}} f(x)\| > \varepsilon\right) \rightarrow 0.$$

Take $\varepsilon = \delta$. Then with probability tending to 1 as $N \rightarrow \infty$, we have

$$\sup_{x \in \mathcal{U}} \|\nabla_{\mathbb{H}} \hat{f}_{\sigma_N}(x) - \nabla_{\mathbb{H}} f(x)\| < \delta.$$

On this event, for all $x \in \mathcal{C}$,

$$\|\nabla_{\mathbb{H}} \hat{f}_{\sigma_N}(x)\| \geq \|\nabla_{\mathbb{H}} f(x)\| - \delta \geq 2\delta - \delta = \delta > 0,$$

using (27). Thus, with probability tending to 1, the empirical density \hat{f}_{σ_N} has no critical point in \mathcal{C} , and all its critical points in \mathcal{U} must lie inside \mathcal{B} . Near each m_j , the nondegenerate critical point property for f and the uniform convergence (26) allow us to invoke the same stability argument as in Lemma 3 (now with f as the population target and \hat{f}_{σ_N} as the empirical estimator). This shows:

- (i) For each j , with probability tending to 1, there exists a unique critical point \hat{m}_j^N of \hat{f}_{σ_N} inside B_j .
- (ii) Moreover,

$$d_{\mathbb{H}}(\hat{m}_j^N, m_j) \xrightarrow[N \rightarrow \infty]{\mathbb{P}} 0.$$

Let $\hat{\mathcal{M}}_{\sigma_N}$ denote the set of all critical points of \hat{f}_{σ_N} in \mathcal{U} . By the previous step, with probability tending to 1 we have,

$$\hat{\mathcal{M}}_{\sigma_N} = \{\hat{m}_1^N, \dots, \hat{m}_K^N\},$$

with each \hat{m}_j^N lying in B_j and converging in probability to m_j .

Define the Hausdorff distance between the finite sets $\hat{\mathcal{M}}_{\sigma_N}$ and \mathcal{M} by,

$$\begin{aligned} d_{\mathbb{H}}(\hat{\mathcal{M}}_{\sigma_N}, \mathcal{M}) &:= \max \left\{ \sup_{\hat{m} \in \hat{\mathcal{M}}_{\sigma_N}} \inf_{m \in \mathcal{M}} d_{\mathbb{H}}(\hat{m}, m), \right. \\ &\quad \left. \sup_{m \in \mathcal{M}} \inf_{\hat{m} \in \hat{\mathcal{M}}_{\sigma_N}} d_{\mathbb{H}}(\hat{m}, m) \right\}. \end{aligned}$$

$$d_{\mathbb{H}}(\hat{\mathcal{M}}_{\sigma_N}, \mathcal{M}) = \max_{1 \leq j \leq K} d_{\mathbb{H}}(\hat{m}_j^N, m_j).$$

Since $K < \infty$ and $d_{\mathbb{H}}(\hat{m}_j^N, m_j) \rightarrow 0$ in probability for each j , it follows by a union bound [35] that

$$d_{\mathbb{H}}(\hat{\mathcal{M}}_{\sigma_N}, \mathcal{M}) \xrightarrow[N \rightarrow \infty]{\mathbb{P}} 0.$$

This shows that, under the bandwidth conditions $\sigma_N \rightarrow 0$ and $N\sigma_N^p \rightarrow \infty$, the estimated centroids $\hat{\mathcal{M}}_{\sigma_N}$ converge in probability to the true set of modes of f . Since HypeGBMS converges algorithmically to empirical modes, the centroids are statistically consistent for the true population modes. \square

9 Experiments

9.1 Details of the Datasets.

We validate the efficacy of HypeGBMS on 11 real-world datasets. Iris, Glass, Ecoli, Wine, Wisconsin B.C, Phishing URL, Abalone, Glass, Zoo, ORHD (Optical Recognition of Handwritten Digits) datasets are taken from the UCI machine learning repository [38]; Flights, MNIST, Pendigits, ORL face datasets are taken from Kaggle.

Table 1: Comparison of Clustering Performance across multiple methods, k -means, GMS, GBMS, DBSCAN, Spectral, GMM, QuickMeanShift, WBMS, Grid-shift, HSFC with our proposed HypeGBMS on 11 Real-world datasets, presented. The best and second-best results are highlighted in boldface and underlined, respectively.

Dataset	Metric	k -means	GMS	GBMS	GMM	DBSCAN	Spectral	QuickMeanShift	WBMS	Gridshift	HSFC	HypeGBMS (Ours)
Iris	ARI	0.742	0.563	0.568	0.507	0.518	0.418	0.701	0.568	0.714	0.621	0.755
	NMI	<u>0.767</u>	0.717	0.734	0.614	0.626	0.509	0.712	0.733	0.754	0.663	0.794
Glass	ARI	0.168	0.187	0.261	0.205	0.225	0.142	0.256	0.157	0.234	0.258	0.281
	NMI	0.306	0.361	<u>0.438</u>	0.361	0.358	0.265	0.427	0.238	0.314	0.428	0.477
Ecoli	ARI	0.384	0.661	0.669	0.637	0.435	0.391	0.354	0.038	0.484	0.431	0.673
	NMI	0.534	0.626	<u>0.631</u>	0.614	0.437	0.592	0.513	0.112	0.515	0.565	0.635
Wine	ARI	0.352	0.103	0.562	0.398	0.329	0.881	0.166	0.802	0.216	0.371	0.813
	NMI	0.423	0.346	0.588	0.585	0.419	<u>0.860</u>	0.319	0.795	0.354	0.429	0.838
Wisconsin B.C.	ARI	0.244	0.667	0.725	0.265	0.297	0.871	0.644	0.679	0.454	0.718	0.882
	NMI	0.402	0.469	0.661	0.362	0.456	<u>0.783</u>	0.546	0.584	0.473	0.742	0.801
Zoo	ARI	0.714	0.544	0.794	0.674	0.515	0.513	0.338	0.751	0.442	0.499	0.807
	NMI	0.771	0.614	<u>0.821</u>	0.789	0.678	0.746	0.526	0.784	0.578	0.717	0.846
Phishing (5K)	ARI	0.001	0.441	0.499	0.392	0.005	0.625	0.224	0.102	0.374	0.121	0.921
	NMI	0.002	0.594	0.401	0.543	0.011	<u>0.597</u>	0.371	0.128	0.387	0.145	0.866
MNIST (5K)	ARI	0.235	0.361	0.142	0.269	0.141	0.392	0.314	0.001	0.218	0.361	0.584
	NMI	0.381	0.465	0.165	0.411	0.278	<u>0.503</u>	0.401	0.002	0.294	0.489	0.701
ORHD	ARI	0.281	0.342	0.517	0.358	0.109	0.535	0.155	0.001	0.164	0.257	0.593
	NMI	0.334	0.421	0.661	0.561	0.259	<u>0.632</u>	0.358	0.004	0.315	0.551	0.702
ORL	ARI	0.341	0.413	0.517	0.358	0.406	0.535	0.427	0.361	0.315	0.561	0.568
	NMI	0.385	0.512	0.591	0.561	0.484	<u>0.632</u>	0.628	0.432	0.377	<u>0.641</u>	0.653
Pendigits	ARI	0.538	0.499	0.577	0.639	0.158	0.580	0.257	0.121	0.253	0.523	0.667
	NMI	0.673	0.681	0.714	<u>0.754</u>	0.312	0.717	0.393	0.336	0.402	0.706	0.776

9.2 Experimental Setup & Baselines.

The performance of HypeGBMS is evaluated using two well-known performance metrics: the Adjusted Rand Index (ARI) [39] and the Normalized Mutual Information (NMI) [40]. The notable base methods, namely k -means [1], Gaussian Mean Shift (GMS) [10], GBMS [41], GMM [42], DBSCAN [8], Spectral [2], along with the State-of-the-Art methods like QuickMeanshift [43], WBMS [13], GridShift [44], HSFC [45] clustering methods, are considered for comparison with our proposed HypeGBMS method. A brief description of the data sets used for the experimentation is given below.

We demonstrate the effectiveness of the proposed framework using the Berkeley Segmentation Data Set (BSDS500) [46], and the PASCAL VOC 2012 dataset [47]. We utilize the four metrics: Segmentation Covering (SC), Probabilistic Rand Index (PRI) [48], Variation of Information (VoI) [49], and F1-Score [50] to compare the results quantitatively. Considering the SC, PRI, and F1-score, higher values represent better results. For VoI, lower values denote better segmentation.

Table 2: Quantitative Results on the BSDS500 [46] dataset across multiple methods, *k*-means, GMS, GBMS, DBSCAN, Spectral, GMM, QuickMeanShift, WBMS, Grid-shift, HSFC with our proposed HypeGBMS.

Methods	Venue	SC	Vol	F1-Score
<i>k</i> -means (Kanungo et al. [1])	[TPAMI'02]	0.1785	2.6851	0.1611
GMS (Cheng [10])	[TPAMI'95]	0.1968	3.0024	0.1636
GBMS (Carreira-Perpinán [11])	[ICML'06]	0.1984	2.9714	0.1825
GMM (Reynolds et al. [6])	[Encycl. Biom'09]	0.2165	2.2932	0.2106
DBSCAN (Khan et al. [8])	[ICADIWT'14]	0.2247	2.1643	0.2993
Spectral (Von Luxburg [2])	[Stat. Comp'07]	0.2081	2.2521	0.2611
WBMS (Chakraborty et al. [13])	[AAAI'21]	0.1833	2.6668	0.3129
QuickMeanShift (Kumar et al. [43])	[AAAI'23]	0.1665	3.0456	0.2784
Gridshift (Kumar et al. [44])	[CVPR'22]	0.2016	2.9814	0.2997
HSFC (Xavier [45])	[PR'10]	0.2036	2.2341	0.2774
HypeGBMS (Ours)		0.2305	2.0441	0.3358

9.3 Experiment on Datasets.

We carried out our experiments on 11 Real-world datasets. The performance noted in Table 1 shows that our proposed method, HypeGBMS, outperforms almost all competitors in terms of ARI and NMI.

Table 3: Quantitative Results on PASCAL VOC 2012 [47] dataset across multiple methods, *k*-means, GMS, GBMS, DBSCAN, Spectral, GMM, QuickMeanShift, WBMS, Grid-shift, HSFC with our proposed HypeGBMS.

Methods	Venue	PRI	Vol	F1-Score
<i>k</i> -means (Kanungo et al. [1])	[TPAMI'02]	0.4001	0.9285	0.5845
GMS (Cheng [10])	[TPAMI'95]	0.3755	1.1951	0.5969
GBMS (Carreira-Perpinán [11])	[ICML'06]	0.3977	1.2514	0.6124
GMM (Reynolds [42])	[Encycl. Biom'09]	0.4019	0.9087	0.6187
DBSCAN (Khan et al. [8])	[ICADIWT'14]	0.4112	0.9142	0.5832
Spectral (Von Luxburg [2])	[Stat Comp'07]	0.3971	0.9566	0.6194
WBMS (Chakraborty et al. [13])	[AAAI'21]	0.3881	1.0231	0.5158
QuickMeanShift (Kumar et al. [43])	[AAAI'23]	0.3645	1.1456	0.5874
Gridshift (Kumar et al. [44])	[CVPR'22]	0.4015	1.1671	0.6148
HSFC (Xavier [45])	[PR'10]	0.3614	1.2045	0.5236
HypeGBMS (Ours)		0.4296	0.8848	0.6388

We have evaluated our proposed method, HypeGBMS, on the BSDS500 & PASCAL VOC 2012 datasets and compared its performance with the other contender methods. We use SC, Vol, F1-Score for the BSDS500 dataset and PRI, Vol, and F1-Score for the PASCAL VOC 2012 dataset. Table 2 shows the quantitative results on the BSDS500 dataset. Table 3 shows the quantitative performance of different indices on the methods in the PASCAL VOC 2012 dataset. The performances in both tables demonstrate that our proposed method, HypeGBMS, outperforms almost all its contenders in terms of SC, PRI, Vol, and F1-Score.

The experimental results on the Phishing dataset in Table 4 clearly show that HypeGBMS outperforms all other clustering methods. HypeGBMS consistently achieves the highest ARI and NMI scores across both data scales (1k and 5k), demonstrating its strong ability to capture the underlying cluster structure. Traditional mean-shift variants such as GMS, GBMS, QuickMeanShift, and Grid Shift show moderate to low accuracy despite reasonable computation times, underscoring their limitations on this dataset. Hyperbolic and graph-based methods like WBMS, and HSFC tend to be less accurate or slower. In contrast, HypeGBMS provides an excellent balance, achieving the best clustering quality while maintaining computational efficiency, making it the most effective method among all these methods.

9.4 Experiments with Image Segmentation.

We have performed experiments on our proposed method, HypeGBMS, with other contenders for image segmentation on some images of the BSDS500[46] datasets, shown in the Figure 2. Similarly, we also done the same experiment on the PASCAL VOC 2012[47] dataset, shown in the Figure 3. Comparative analysis was performed using benchmark datasets, where we carefully measured segmentation accuracy and robustness under varying conditions. Across all evaluation metrics, our method consistently outperformed competing techniques, demonstrating superior boundary preservation, higher segmentation accuracy, and improved adaptability to complex structures. These results clearly highlight the strength of our approach and its potential to advance the state-of-the-art methods in image segmentation tasks.

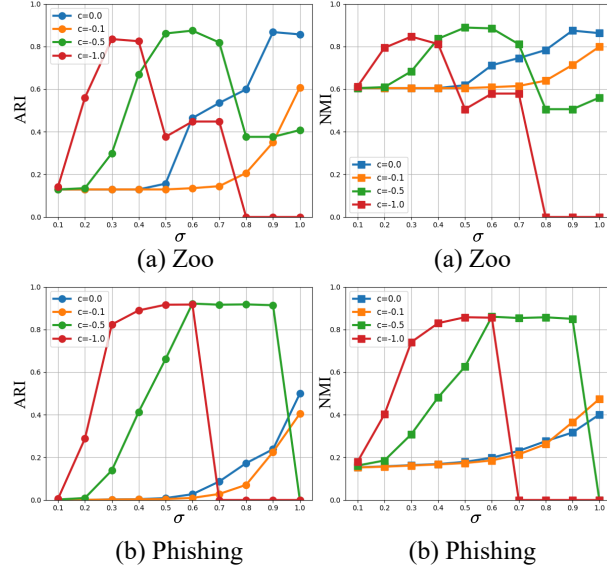


Fig. 4: The performance metrics (ARI, NMI) vs bandwidth (σ) plots for different values of curvature (c) for our proposed HypeGBMS for two real-world datasets: (a) Zoo, (b) Phishing URL, respectively.

Table 4: Clustering performance comparison with runtime on Phishing dataset(for 1k and 5k samples).

Dataset	Method	N	Time (sec)	ARI	NMI
Phishing	GBMS	1k	0.216	0.514	0.464
		5k	1.011	0.499	0.401
	GMS	1k	0.326	0.492	0.622
		5k	1.263	0.441	0.594
	QuickMeanShift	1k	0.455	0.286	0.423
		5k	1.994	0.224	0.371
Phishing	Grid Shift	1k	0.664	0.406	0.414
		5k	2.624	0.374	0.387
	WBMS	1k	1.124	0.141	0.186
		5k	4.821	0.102	0.128
	HSFC	1k	0.471	0.148	0.197
		5k	2.254	0.121	0.145
HypeGBMS (Ours)		1k	0.464	0.912	0.842
		5k	2.124	0.921	0.866

9.5 Ablation Study

We conducted an ablation study by varying the two key parameters (i) the bandwidth of the Gaussian kernel (σ), (ii) the curvature of the Poincaré disc (c).

Choice of bandwidth of Gaussian Kernel. We have experimented on the performance metrics, ARI, NMI, with the bandwidth parameter (σ) varying from 0.1 to 1.0 for the different curvature values (c)

$\{0.0, -0.1, -0.5, -1.0\}$ for two real datasets, Zoo and Phishing URL, respectively in Figure 4. The plots show that for higher curvature values (c) such as $c = -0.5, -1.0$; optimal performance is achieved for bandwidth parameters (σ) lying within the range of 0.4 to 0.6.

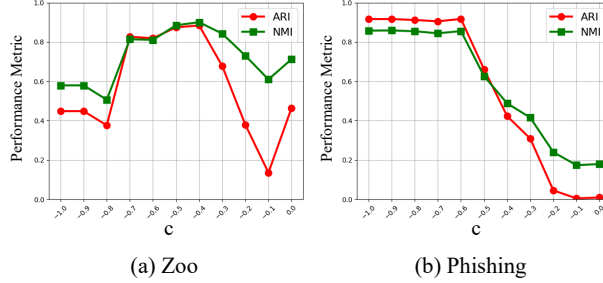


Fig. 5: The Performance metrics, ARI, NMI vs curvature (c) for our proposed method HypeGBMS for two real-world datasets (a) Zoo, (b) Phishing URL, respectively.

Table 5: ARI for our proposed method, *HypeGBMS* trained on Phishing dataset with different curvature c .

Curvature (c)	-0.1	-0.2	-0.3	-0.4	-0.5
ARI	0.084	0.109	0.358	0.426	0.751
Curvature (c)	-0.6	-0.7	-0.8	-0.9	-1.0
ARI	0.921	0.886	0.918	0.911	0.894

Choice of Curvature of the Poincaré disc. We have performed an experiment on the performance metrics (ARI, NMI) with the curvature (c) varying from -1.0 to 0.0 , fixing the bandwidth (σ) value 0.6 on the two real datasets, Zoo and Phishing URL, respectively shown in Figure 5. Table 5 shows the values for the performance metric, ARI, for different curvatures from -1.0 to -0.1 on the Phishing dataset. The optimal performance is achieved when the curvature value (c) is equal to -0.6 .

10 Conclusion & Future Works

Our proposed method, HypeGBMS, a hyperbolic extension of the Gaussian Blurring Mean Shift algorithm, is designed to overcome the limitations of Euclidean clustering methods on hierarchical and tree-structured data. By embedding data in the Poincaré ball and employing Möbius weighted means for mode updates, our method preserves the intrinsic geometry of hyperbolic space while retaining the density-seeking behavior of mean-shift clustering. Theoretical analysis established convergence properties and computational feasibility, while empirical evaluations confirmed that HypeGBMS provides superior performance on datasets where Euclidean approaches struggle. Beyond clustering accuracy, the ability of hyperbolic geometry to efficiently represent hierarchical relationships highlights the broader potential of our framework for tasks in complex network analysis and representation learning.

Extending HypeGBMS to large-scale datasets through efficient approximation schemes and parallelization strategies would further broaden its applicability. Another promising direction is the development of adaptive mechanisms for selecting curvature parameters, integrating the method with modern hyperbolic deep learning architectures.

A Appendix

This Appendix provides the necessary proofs for the Convergence Analysis in Section 7 of our proposed HypeGBMS method. Let $(\mathcal{M}, g) = (\mathbb{D}_c^p, g_c)$ be the p -dimensional Poincaré ball with sectional curvature $c = -\kappa < 0$ and hyperbolic distance $d_{\mathbb{H}}$.

A.1 Comparison bound

The key geometric input is a pointwise bound on the Hessian of the squared-distance function. Define, for $s \geq 0$,

$$g_c(s) := \begin{cases} \sqrt{\kappa} s \coth(\sqrt{\kappa} s), & \kappa > 0 \text{ (i.e. } c < 0\text{),} \\ 1, & \kappa = 0. \end{cases}$$

Note $g_c(s) \geq 1$ for $s \geq 0$, and $g_c(s) \rightarrow 1$ as $\kappa \rightarrow 0$.

Lemma 4 (Distance-square Hessian bound) For any fixed $y \in \mathcal{U}$ the function $\phi_y(x) := \frac{1}{2}d_{\mathbb{H}}^2(x, y)$ is \mathbb{C}^2 on $\mathcal{U} \setminus \{y\}$ and for every $x \in \mathcal{U}$ and tangent vector $v \in T_x \mathcal{M}$,

$$\text{Hess}_x\left(\frac{1}{2}d_{\mathbb{H}}^2(\cdot, y)\right)[v, v] \leq g_c(d_{\mathbb{H}}(x, y)) \|v\|_g^2.$$

Consequently, for any $u \in T_x \mathcal{M}$ small enough that $\exp_x(u) \in \mathcal{U}$,

$$d_{\mathbb{H}}^2(\exp_x(u), y) \leq d_{\mathbb{H}}^2(x, y) - 2\langle u, \log_x y \rangle + G \|u\|_g^2, \quad (28)$$

where $G := \sup_{s \in [0, D]} g_c(s) < \infty$.

Proof Since (\mathcal{M}, g) is a Hadamard manifold, the exponential map at any point is a global diffeomorphism, and there is no cut locus. In particular, the distance function $x \mapsto d_{\mathbb{H}}(x, y)$ is smooth on $\mathcal{M} \setminus \{y\}$. Therefore ϕ_y is \mathbb{C}^2 on $\mathcal{U} \setminus \{y\}$. Let $r(x) := d_{\mathbb{H}}(x, y)$ denote the hyperbolic distance to y . On a manifold with sectional curvature bounded below by $-\kappa$, the Hessian comparison theorem (see, e.g., [51, Ch. 5]) states that for all $x \neq y$ and $v \in T_x \mathcal{M}$,

$$\text{Hess}_x r[v, v] \leq \sqrt{\kappa} \coth(\sqrt{\kappa} r(x)) (\|v\|_g^2 - \langle \nabla r(x), v \rangle^2), \quad (29)$$

with the convention that for $\kappa = 0$ the right-hand side is simply $\|v\|_g^2 - \langle \nabla r(x), v \rangle^2$ (since then r is Euclidean distance). Here $\nabla r(x)$ denotes the Riemannian gradient of r at x , a unit vector pointing along the geodesic from x to y .

We now express, $\text{Hess}_x(\phi_y)$ in terms of r and $\text{Hess}_x r$. Recall that

$$\phi_y(x) = \frac{1}{2}r(x)^2.$$

Thus, for any $v \in T_x \mathcal{M}$,

$$\begin{aligned} \text{Hess}_x \phi_y[v, v] &= \text{Hess}_x\left(\frac{1}{2}r^2\right)[v, v] \\ &= \frac{1}{2} \text{Hess}_x(r^2)[v, v] \\ &= \frac{1}{2}(2r(x) \text{Hess}_x r[v, v] + 2\langle \nabla r(x), v \rangle^2) \\ &= r(x) \text{Hess}_x r[v, v] + \langle \nabla r(x), v \rangle^2. \end{aligned}$$

Using (29), for $\kappa > 0$ we obtain

$$\begin{aligned} \text{Hess}_x \phi_y[v, v] &\leq r(x) \sqrt{\kappa} \coth(\sqrt{\kappa} r(x)) (\|v\|_g^2 - \langle \nabla r(x), v \rangle^2) + \langle \nabla r(x), v \rangle^2 \\ &= g_c(r(x)) \|v\|_g^2 + (1 - g_c(r(x))) \langle \nabla r(x), v \rangle^2, \end{aligned}$$

where $g_c(s) = \sqrt{\kappa} s \coth(\sqrt{\kappa} s)$ for $s \geq 0$. Since $g_c(s) \geq 1$ for all $s \geq 0$, the coefficient $1 - g_c(r(x)) \leq 0$, hence the second term is nonpositive. Thus,

$$\text{Hess}_x \phi_y[v, v] \leq g_c(r(x)) \|v\|_g^2 = g_c(d_{\mathbb{H}}(x, y)) \|v\|_g^2.$$

For $\kappa = 0$, we have r equal to Euclidean distance, $\text{Hess}_x r[v, v] = \|v\|_g^2 - \langle \nabla r(x), v \rangle^2$, and the same calculation yields $\text{Hess}_x \phi_y[v, v] \leq \|v\|_g^2 = g_c(r(x)) \|v\|_g^2$ with $g_c \equiv 1$. This establishes the Hessian bound

$$\text{Hess}_x\left(\frac{1}{2}d_{\mathbb{H}}^2(\cdot, y)\right)[v, v] \leq g_c(d_{\mathbb{H}}(x, y)) \|v\|_g^2. \quad (30)$$

Let $x \in \mathcal{U}$ and $u \in T_x \mathcal{M}$ be such that $\exp_x(u) \in \mathcal{U}$. Consider the unit-speed geodesic

$$\gamma : [0, 1] \rightarrow \mathcal{M}, \quad \gamma(t) := \exp_x(tu),$$

so that $\gamma(0) = x$, $\gamma(1) = \exp_x(u)$ and $\dot{\gamma}(t) = u$ for all t (with $\|u\|_g$ constant). Define the scalar function

$$\psi(t) := \phi_y(\gamma(t)) = \frac{1}{2}d_{\mathbb{H}}^2(\gamma(t), y).$$

Then

$$\begin{aligned} \psi'(t) &= \langle \nabla \phi_y(\gamma(t)), \dot{\gamma}(t) \rangle, \\ \psi''(t) &= \text{Hess}_{\gamma(t)} \phi_y[\dot{\gamma}(t), \dot{\gamma}(t)]. \end{aligned}$$

Using the Hessian bound from (30) and the fact that $\|\dot{\gamma}(t)\|_g = \|u\|_g$, we obtain

$$\psi''(t) \leq g_c(d_{\mathbb{H}}(\gamma(t), y)) \|u\|_g^2.$$

Let $D := \sup\{d_{\mathbb{H}}(z, y) : z \in \mathcal{U}\}$; since \mathcal{U} is a bounded geodesic ball, $D < \infty$, and we may define

$$G := \sup_{s \in [0, D]} g_c(s) < \infty.$$

Then, for all $t \in [0, 1]$,

$$\psi''(t) \leq G \|u\|_g^2.$$

Integrating this differential inequality twice yields a second-order upper bound. Integrate from 0 to 1:

$$\psi'(1) - \psi'(0) = \int_0^1 \psi''(t) dt \leq G \|u\|_g^2.$$

Integrating once more,

$$\begin{aligned} \psi(1) - \psi(0) &= \int_0^1 \psi'(t) dt \\ &= \psi'(0) + \int_0^1 (1-t) \psi''(t) dt \leq \psi'(0) + \frac{G}{2} \|u\|_g^2. \end{aligned}$$

We compute $\psi'(0)$. Using $\phi_y(x) = \frac{1}{2}d_{\mathbb{H}}^2(x, y)$ and the standard identity $\nabla_x \phi_y(x) = -\log_x y$, we obtain

$$\psi'(0) = \langle \nabla \phi_y(x), u \rangle = -\langle \log_x y, u \rangle.$$

Therefore,

$$\psi(1) \leq \psi(0) - \langle \log_x y, u \rangle + \frac{G}{2} \|u\|_g^2.$$

Recalling that $\psi(t) = \frac{1}{2}d_{\mathbb{H}}^2(\gamma(t), y)$ and $\gamma(1) = \exp_x(u)$, this inequality becomes

$$\frac{1}{2}d_{\mathbb{H}}^2(\exp_x(u), y) \leq \frac{1}{2}d_{\mathbb{H}}^2(x, y) - \langle \log_x y, u \rangle + \frac{G}{2} \|u\|_g^2.$$

Multiplying both sides by 2 yields

$$d_{\mathbb{H}}^2(\exp_x(u), y) \leq d_{\mathbb{H}}^2(x, y) - 2\langle u, \log_x y \rangle + G \|u\|_g^2,$$

which is exactly (28).

This completes the proof of the lemma. \square

A.2 Möbius weighted mean is a first-order retraction

The HypeGBMS update implements a Möbius-weighted mean. For local analysis, we replace it with the exponential step. This is justified because the Möbius operations on the Poincaré ball provide a smooth retraction whose first-order Taylor expansion coincides with the exponential map. Below we state a precise local approximation.

Lemma 5 (Retraction approximation of Möbius mean) Let $x \in \mathcal{U}$ and let $\{x_j\}$ be points in \mathcal{U} with weights $\{w_j\}$, $\sum_j w_j = 1$, and let \bar{x}_M denote the Möbius-weighted mean used in the Algorithm 2. Let $v^* := \sum_j w_j \log_x x_j \in T_x \mathcal{M}$. Then, for $\max_j d_{\mathbb{H}}(x, x_j)$ sufficiently small,

$$\log_x(\bar{x}_M) = v^* + R, \quad \|R\|_g = \mathcal{O}\left(\max_j d_{\mathbb{H}}(x, x_j)^3\right),$$

so in particular $\bar{x}_M = \exp_x(v^*) + \mathcal{O}(\|v^*\|^3)$.

Proof We set $v_j = \log_x(x_j) \in T_x(\mathbb{D}_c^p)$. Assume $\|v_j\|_g$ are sufficiently small.

Define the Möbius weighted mean $\bar{x}_M = \bigoplus_j w_j \otimes_c x_j$ and note that in the tangent chart

$$\log_x(\bar{x}_M) = \sum_j w_j v_j + R(x, \{v_j\}, c), \quad (31)$$

where $\|R(x, \{v_j\}, c)\|_g = \mathcal{O}(\max_j \|v_j\|_g^3)$. In normal coordinates, the exponential map satisfies $\exp_x(v) = x + v + \mathcal{O}(\|v\|^3)$ since the Christoffel symbols vanish at x . Hence the exponential update $\bar{x}_{\text{exp}} = \exp_x(\sum_j w_{ij} v_j)$ shares the same first and second differential terms. Consequently,

$$\log_x(\bar{x}_M) = \sum_j w_j v_j + \mathcal{O}(\|v_j\|^3), \quad (32)$$

$$\bar{x}_M = \exp_x\left(\sum_j w_j v_j\right) + \mathcal{O}(\|v_j\|^3). \quad (33)$$

Therefore, the Möbius weighted mean defines a smooth retraction at x whose differential at the origin equals the identity, establishing its first-order equivalence with the Riemannian exponential map. \square

A.3 Approximation Between Möbius and Fréchet Mean

Proposition 1 Let $\{x_j\}_{j=1}^N \subset \mathbb{D}_c^p$ lie within a geodesic ball $B_{\mathbb{H}}(x_0, r)$ of radius $r < 1$ and curvature magnitude $\kappa = -c > 0$. Then there exists a constant $C_p > 0$, depending only on dimension p , such that

$$d_{\mathbb{H}}(\bar{x}_M, \bar{x}_F) \leq C_p \kappa r^3. \quad (34)$$

Moreover, $\bar{x}_M, \bar{x}_F \in B_{\mathbb{H}}(x_0, r)$.

Proof Let $\xi_j = \log_{x_0}(x_j) \in T_{x_0}\mathcal{M}$ with $\|\xi_j\| \leq r$.

(\mathcal{M}, g) be the p -dimensional Poincaré ball with constant sectional curvature $\kappa = -c > 0$, and let

$$F(z) := \sum_{j=1}^N w_j d_{\mathbb{H}}^2(z, x_j),$$

For each fixed x_j , define

$$\psi_j(z) := \frac{1}{2} d_{\mathbb{H}}^2(z, x_j).$$

A standard result in Riemannian geometry states that,

$$\nabla_z \psi_j(z) = -\log_z(x_j), \quad \text{Hess}_z \psi_j \text{ is smooth.}$$

Since $d_{\mathbb{H}}^2(z, x_j) = 2\psi_j(z)$, we obtain

$$\nabla F(z) = \sum_{j=1}^N w_j \nabla_z d_{\mathbb{H}}^2(z, x_j) = -2 \sum_{j=1}^N w_j \log_z(x_j),$$

and similarly,

$$\text{Hess}_z F = 2 \sum_{j=1}^N w_j \text{Hess}_z \left(\frac{1}{2} d_{\mathbb{H}}^2(\cdot, x_j) \right).$$

Since (\mathcal{M}, g) has constant curvature κ , thus by [51, Ch. 5]) we have

$$\left\| \text{Hess}_z \left(\frac{1}{2} d_{\mathbb{H}}^2(\cdot, x_j) \right) - I \right\| \leq \frac{\kappa}{3} d_{\mathbb{H}}^2(z, x_j). \quad (35)$$

Assuming all relevant points lie in a geodesic ball of radius $r < 1$, we have $d_{\mathbb{H}}(z, x_j) \leq r$, and hence

$$\left\| \text{Hess}_z \left(\frac{1}{2} d_{\mathbb{H}}^2(\cdot, x_j) \right) - I \right\| \leq \frac{\kappa r^2}{3}.$$

Let $\exp_{x_0} : T_{x_0}\mathcal{M} \rightarrow \mathcal{M}$ be the exponential map and denote by $\xi, \xi_j \in T_{x_0}\mathcal{M} \cong \mathbb{R}^p$ the normal coordinates of z and x_j , respectively:

$$z = \exp_{x_0}(\xi), \quad x_j = \exp_{x_0}(\xi_j), \quad \|\xi\|, \|\xi_j\| \leq r.$$

Define

$$f_j(\xi) := \frac{1}{2} d_{\mathbb{H}}^2(\exp_{x_0}(\xi), x_j).$$

Then in these coordinates,

$$\nabla_{\xi} f_j(0) = -\log_{x_0}(x_j) = -\xi_j.$$

Using the integral form of the Taylor expansion,

$$\nabla_{\xi} f_j(\xi) = \nabla_{\xi} f_j(0) + \int_0^1 \text{Hess}_{\xi} f_j(t\xi)[\xi] dt.$$

From (35), there exists a matrix-valued function $E_j(t\xi)$ with

$$\text{Hess}_{\xi} f_j(t\xi) = I + E_j(t\xi), \quad \|E_j(t\xi)\| \leq \frac{\kappa r^2}{3}.$$

Therefore,

$$\nabla_{\xi} f_j(\xi) = -\xi_j + \int_0^1 (I + E_j(t\xi))[\xi] dt = -\xi_j + \xi + R_j(\xi),$$

where

$$R_j(\xi) := \int_0^1 E_j(t\xi)[\xi] dt \implies \|R_j(\xi)\| \leq \frac{\kappa r^2}{3} \|\xi\| \leq \frac{\kappa r^3}{3}$$

Since $F(z) = 2 \sum_j w_j f_j(\xi)$, we obtain

$$\begin{aligned} \nabla_{\xi} F(\exp_{x_0}(\xi)) &= 2 \sum_{j=1}^N w_j \nabla_{\xi} f_j(\xi) \\ &= 2 \sum_{j=1}^N w_j (-\xi_j + \xi + R_j(\xi)). \end{aligned}$$

Rearranging,

$$\nabla F(\exp_{x_0}(\xi)) = 2\left(\xi - \sum_{j=1}^N w_j \xi_j\right) + R_F(\xi), \quad (36)$$

where

$$R_F(\xi) := 2 \sum_{j=1}^N w_j R_j(\xi),$$

$$\|R_F(\xi)\| \leq 2 \sum_{j=1}^N w_j \|R_j(\xi)\| \leq \frac{2}{3} \kappa r^3 = C_1 \kappa r^3.$$

Let $\bar{x}_F = \exp_{x_0}(\xi_F)$. Since $\nabla F(\bar{x}_F) = 0$, substituting $\xi = \xi_F$ into (36) gives

$$0 = 2\left(\xi_F - \sum_j w_j \xi_j\right) + R_F(\xi_F),$$

hence

$$\xi_F = \sum_{j=1}^N w_j \xi_j - \frac{1}{2} R_F(\xi_F).$$

Defining $\Delta_F := \xi_F - \sum_j w_j \xi_j$, we obtain

$$\Delta_F = -\frac{1}{2} R_F(\xi_F) \quad \|\Delta_F\| \leq \frac{1}{2} \|R_F(\xi_F)\| \leq \frac{1}{2} C_1 \kappa r^3.$$

Finally, from the bound

$$\text{Hess}_{x_0} F = 2I + \mathcal{O}(\kappa r^2),$$

we see that for r sufficiently small, F is strictly geodesically convex in $B_{\mathbb{H}}(x_0, r)$, implying uniqueness and smoothness of the minimizer \bar{x}_F .

For the Möbius mean, note that the Möbius exponential and logarithmic maps are related to the Riemannian exponential and logarithm by (see [52, Sec 7.1], [53, Eq. (5)])

$$\exp_{x_0}(v) = x_0 \oplus_c v = \exp_{x_0}\left(v - \frac{\kappa}{6} \|v\|^2 v + \mathcal{O}(\kappa^2 r^4)\right),$$

$$\log_{x_0}(x_j) = \xi_j - \frac{\kappa}{6} \|\xi_j\|^2 \xi_j + \mathcal{O}(\kappa^2 r^4).$$

Consequently, in tangent coordinates, the Möbius weighted mean is given by

$$\begin{aligned} \xi_M &= \sum_j w_j \log_{x_0}(x_j) \\ &= \sum_j w_j \xi_j - \frac{\kappa}{6} \sum_j w_j \|\xi_j\|^2 \xi_j + \mathcal{O}(\kappa^2 r^4). \end{aligned} \quad (37)$$

Subtracting the two expansions $\xi_F = \sum_j w_j \xi_j + \Delta_F$ and (37), one obtains

$$\xi_F - \xi_M = \frac{\kappa}{6} \sum_j w_j \|\xi_j\|^2 \xi_j + \Delta_F + \mathcal{O}(\kappa^2 r^4),$$

and therefore, by the triangle inequality,

$$\|\xi_F - \xi_M\| \leq \frac{\kappa}{6} \sum_j w_j \|\xi_j\|^3 + \|\Delta_F\| + \mathcal{O}(\kappa^2 r^4) \leq C_p \kappa r^3,$$

where $C_p = \frac{1}{6} + C_1 + \mathcal{O}(\kappa r)$ depends only on p through curvature tensor bounds.

To convert this tangent-space bound into a bound in the manifold, recall that for $\xi_1, \xi_2 \in T_{x_0} \mathcal{M}$ with $\|\xi_1\|, \|\xi_2\| \leq r$, the Riemannian distance and tangent-norm satisfy (see [51, Prop. 6.2])

$$|d_{\mathbb{H}}(\exp_{x_0}(\xi_1), \exp_{x_0}(\xi_2)) - \|\xi_1 - \xi_2\|| \leq C_3 \kappa r^3.$$

Applying this to ξ_F and ξ_M gives

$$d_{\mathbb{H}}(\bar{x}_F, \bar{x}_M) \leq \|\xi_F - \xi_M\| + C_3 \kappa r^3 \leq C_p \kappa r^3,$$

Finally, since $\|\xi_F\|, \|\xi_M\| \leq r + \mathcal{O}(\kappa r^3)$ and the injectivity radius of \mathbb{D}_c^p is infinite, both \bar{x}_F and \bar{x}_M lie within $B_{\mathbb{H}}(x_0, r)$, which completes the proof. \square

References

- [1] Kanungo, T., Mount, D.M., Netanyahu, N.S., Piatko, C.D., Silverman, R., Wu, A.Y.: An efficient k-means clustering algorithm: Analysis and implementation. *IEEE transactions on pattern analysis and machine intelligence* **24**(7), 881–892 (2002)
- [2] Von Luxburg, U.: A tutorial on spectral clustering. *Statistics and computing* **17**, 395–416 (2007)
- [3] Dhillon, I.S., Guan, Y., Kulis, B.: Kernel k-means: spectral clustering and normalized cuts. In: *Proceedings of the Tenth ACM SIGKDD International Conference on Knowledge Discovery and Data Mining*, pp. 551–556 (2004)
- [4] Nielsen, F., Nielsen, F.: Hierarchical clustering. *Introduction to HPC with MPI for Data Science*, 195–211 (2016)
- [5] Gowda, K.C., Krishna, G.: Agglomerative clustering using the concept of mutual nearest neighbourhood. *Pattern recognition* **10**(2), 105–112 (1978)
- [6] Reynolds, D.A., et al.: Gaussian mixture models. *Encyclopedia of biometrics* **741**(659-663) (2009)
- [7] Yang, M.-S., Lai, C.-Y., Lin, C.-Y.: A robust em clustering algorithm for gaussian mixture models. *Pattern Recognition* **45**(11), 3950–3961 (2012)
- [8] Khan, K., Rehman, S.U., Aziz, K., Fong, S., Sarasvady, S.: Dbscan: Past, present and future. In: *The Fifth International Conference on the Applications of Digital Information and Web Technologies (ICADIWT 2014)*, pp. 232–238 (2014). IEEE
- [9] McInnes, L., Healy, J., Astels, S., et al.: HdbSCAN: Hierarchical density based clustering. *J. Open Source Softw.* **2**(11), 205 (2017)
- [10] Cheng, Y.: Mean shift, mode seeking, and clustering. *IEEE transactions on pattern analysis and machine intelligence* **17**(8), 790–799 (1995)
- [11] Carreira-Perpinán, M.A.: Fast nonparametric clustering with gaussian blurring mean-shift. In: *Proceedings of the 23rd International Conference on Machine Learning*, pp. 153–160 (2006)
- [12] Carreira-Perpinán, M.A.: A review of mean-shift algorithms for clustering. *arXiv preprint arXiv:1503.00687* (2015)
- [13] Chakraborty, S., Paul, D., Das, S.: Automated clustering of high-dimensional data with a feature weighted mean shift algorithm. In: *Proceedings of the AAAI Conference on Artificial Intelligence*, vol. 35, pp. 6930–6938 (2021)
- [14] Ontrup, J., Ritter, H.: Large-scale data exploration with the hierarchically growing hyperbolic som. *Neural Networks* **19**(6-7), 751–761 (2006)
- [15] Baker, C., Suárez-Méndez, I., Smith, G., Marsh, E.B., Funke, M., Mosher, J.C., Maestú, F., Xu, M., Pantazis, D.: Hyperbolic graph embedding of meg brain networks to study brain alterations in individuals with subjective cognitive decline. *IEEE journal of biomedical and health informatics* **28**(12), 7357–7368 (2024)
- [16] Fang, P., Harandi, M., Lan, Z., Petersson, L.: Poincaré kernels for hyperbolic representations. *International Journal of Computer Vision* (2023)
- [17] Chami, I., Gu, A., Chatziafratis, V.: From trees to continuous embeddings and back: Hyperbolic hierarchical clustering. In: *Advances in Neural Information Processing Systems* (2020)
- [18] Zhao, J., Hao, Y., Rashtchian, C.: Unsupervised embedding of hierarchical structure in euclidean space. *arXiv preprint arXiv:2010.16055* (2020)
- [19] Wei, R., Liu, Y., Song, J., Xie, Y., Zhou, K.: Hyperbolic hierarchical contrastive hashing. *arXiv preprint arXiv:2212.08904* (2022)

[20] Do Carmo, M.P., Flaherty Francis, J.: *Riemannian Geometry* vol. 2. Springer, ??? (1992)

[21] Spivak, M.: *A comprehensive introduction to differential geometry, publish or perish.* Inc., Berkeley **2** (1979)

[22] Lee, J.M.: *Riemannian Manifolds: an Introduction to Curvature* vol. 176. Springer, ??? (2006)

[23] Ungar, A.: *A Gyrovector Space Approach to Hyperbolic Geometry.* Springer, ??? (2022)

[24] Ratcliffe, J.G.: *Hyperbolic n-manifolds. Foundations of Hyperbolic Manifolds*, 508–599 (2006)

[25] Ganea, O., Bécigneul, G., Hofmann, T.: Hyperbolic neural networks. *Advances in neural information processing systems* **31** (2018)

[26] Mishne, G., Wan, Z., Wang, Y., Yang, S.: The numerical stability of hyperbolic representation learning. In: *International Conference on Machine Learning*, pp. 24925–24949 (2023). PMLR

[27] Friedman, J.H., Bentley, J.L., Finkel, R.A.: An algorithm for finding best matches in logarithmic expected time. *ACM Transactions on Mathematical Software* **3**(3), 209–226 (1977)

[28] Omohundro, S.M.: Five balltree construction algorithms. In: *International Joint Conference on Artificial Intelligence*, pp. 50–55 (1989)

[29] Muja, M., Lowe, D.G.: Fast approximate nearest neighbors with automatic algorithm configuration. In: *International Conference on Computer Vision Theory and Applications (VISAPP)* (2009)

[30] Williams, C.K.I., Seeger, M.: Using the nyström method to speed up kernel machines. In: *Advances in Neural Information Processing Systems*, pp. 682–688 (2001)

[31] Rahimi, A., Recht, B.: Random features for large-scale kernel machines. In: *Advances in Neural Information Processing Systems*, pp. 1177–1184 (2007)

[32] Jiang, H., Vondrák, J.: Quickshift++: Provably good initializations for kernel methods. In: *International Conference on Machine Learning*, pp. 2289–2298 (2018)

[33] Afsari, B.: Riemannian l^p center of mass: existence, uniqueness, and convexity. *Proceedings of the American Mathematical Society* **139**(2), 655–673 (2011)

[34] Rudin, W.: *Principles of mathematical analysis.* 3rd ed. (1976)

[35] Wainwright, M.J.: *High-dimensional Statistics: A Non-asymptotic Viewpoint* vol. 48. Cambridge university press, ??? (2019)

[36] Lee, J.M.: *Introduction to Riemannian Manifolds* vol. 2. Springer, ??? (2018)

[37] Pelletier, B.: Kernel density estimation on riemannian manifolds. *Statistics & probability letters* **73**(3), 297–304 (2005)

[38] Dua, D., Graff, C., *et al.*: Uci machine learning repository, 2017. URL <http://archive.ics.uci.edu/ml> **7**(1), 62 (2017)

[39] Santos, J.M., Embrechts, M.: On the use of the adjusted rand index as a metric for evaluating supervised classification. In: *International Conference on Artificial Neural Networks*, pp. 175–184 (2009). Springer

[40] Estévez, P.A., Tesmer, M., Perez, C.A., Zurada, J.M.: Normalized mutual information feature selection. *IEEE Transactions on neural networks* **20**(2), 189–201 (2009)

[41] Carreira-Perpinán, M.A.: Fast nonparametric clustering with gaussian blurring mean-shift. In: *Proceedings of the 23rd International Conference on Machine Learning*, pp. 153–160 (2006)

[42] Reynolds, D.: Gaussian mixture models. In: *Encyclopedia of Biometrics*, pp. 827–832. Springer, ??? (2015)

[43] Kumar, A., Das, S., Mallipeddi, R.: Ueqms: Umap embedded quick mean shift algorithm for high

dimensional clustering. In: Proceedings of the AAAI Conference on Artificial Intelligence, vol. 37, pp. 8386–8395 (2023)

- [44] Kumar, A., Ajani, O.S., Das, S., Mallipeddi, R.: Gridshift: A faster mode-seeking algorithm for image segmentation and object tracking. In: Proceedings of the IEEE/CVF Conference on Computer Vision and Pattern Recognition, pp. 8131–8139 (2022)
- [45] Xavier, A.E.: The hyperbolic smoothing clustering method. *Pattern Recognition* **43**(3), 731–737 (2010)
- [46] Martin, D., Fowlkes, C., Malik, J.: Berkeley segmentation dataset (2002)
- [47] Everingham, M., Eslami, S.A., Van Gool, L., Williams, C.K., Winn, J., Zisserman, A.: The pascal visual object classes challenge: A retrospective. *International journal of computer vision* **111**(1), 98–136 (2015)
- [48] Carpineto, C., Romano, G.: Consensus clustering based on a new probabilistic rand index with application to subtopic retrieval. *IEEE Transactions on Pattern Analysis and Machine Intelligence* **34**(12), 2315–2326 (2012)
- [49] Meilă, M.: Comparing clusterings by the variation of information. In: Learning Theory and Kernel Machines: 16th Annual Conference on Learning Theory and 7th Kernel Workshop, COLT/Kernel 2003, Washington, DC, USA, August 24–27, 2003. Proceedings, pp. 173–187 (2003). Springer
- [50] Sokolova, M., Japkowicz, N., Szpakowicz, S.: Beyond accuracy, f-score and roc: a family of discriminant measures for performance evaluation. In: Australasian Joint Conference on Artificial Intelligence, pp. 1015–1021 (2006). Springer
- [51] Boumal, N.: An Introduction to Optimization on Smooth Manifolds. Cambridge University Press, ??? (2020)
- [52] Ungar, A.A.: Analytic Hyperbolic Geometry and Albert Einstein’s Special Theory of Relativity. World Scientific, ??? (2008)
- [53] Ganea, O.-E., Bécigneul, G., Hofmann, T.: Hyperbolic neural networks. In: Advances in Neural Information Processing Systems (NeurIPS), pp. 5345–5355 (2018)